Magnetic Fields in Molecular Clouds

Richard M. Crutcher

Department of Astronomy, University of Illinois, Urbana, Illinois 61801;
email: crutcher@illinois.edu

Annu. Rev. Astron. Astrophys. 2012. 50:29–63

First published online as a Review in Advance on May 29, 2012

The *Annual Review of Astronomy and Astrophysics* is online at astro.annualreviews.org

This article's doi:
10.1146/annurev-astro-081811-125514

0066-4146/12/0922-0029$20.00

Keywords

ambipolar diffusion, dust polarization, magnetohydrodynamic (MHD) turbulence, spectral-line polarization, star formation, Zeeman effect

Abstract

This review examines observations of magnetic fields in molecular clouds and what those observations tell us about the theory of molecular cloud evolution and star formation. First, the review briefly summarizes classes of theoretical models of molecular clouds and specific predictions of the models that can be tested by observation. Then, the review describes the techniques for observing and mapping magnetic fields in molecular clouds, followed by discussion of important examples of observational studies using each technique. A synthesis of results from all observational techniques summarizes the current state, which is that though magnetic fields generally dominate turbulence, there is no definitive evidence for magnetic fields dominating gravity in molecular clouds or for ambipolar-diffusion-driven star formation. Finally, the review discusses prospects for advances in our observational capabilities with telescopes and instruments now beginning operation or under construction.

1. INTRODUCTION

The origin and evolution of magnetic fields in the Universe is not understood (e.g., Rees 2005). The current picture is that magnetic fields in Galactic molecular clouds are the frozen-in fields from the ISM of the Milky Way, which arose from galactic-scale dynamo amplification of seed fields generated by Biermann batteries in Population III stars and/or in early AGNs.

Although magnetic fields in molecular clouds can be an interesting topic in itself, the most important reason for their study is the role of magnetic fields in the formation and evolution of interstellar clouds and in star formation. This review therefore focuses on that topic. Understanding star formation is a key astrophysical problem; Shu, Adams & Lizano (1987) and McKee & Ostriker (2007) have comprehensively reviewed the field. In spite of significant progress in recent years, there remain unanswered fundamental questions about the basic physics of star formation. In particular, what drives the star-formation process? The two major classes of star-formation theory differ in the role played by magnetic fields. The strong-field models (e.g., Mouschovias 1991, Mouschovias & Ciolek 1999) have magnetic fields controlling the formation and evolution of the molecular clouds from which stars form, with ambipolar diffusion driving the formation of cores and their gravitational collapse to form protostars. The weak-field models (e.g., Padoan & Nordlund 1999, MacLow & Klessen 2004) have turbulent flows controlling the formation of clouds and cores, with cores either dissipating back into the general ISM or collapsing and forming stars if they are self-gravitating when formed. Triggered star formation generally falls into this second class of star-formation theory. More recently, theory and simulation have moved to considering important roles for both turbulent flows and magnetic fields (e.g., Nakamura & Li 2005, Tilley & Pudritz 2007, Kudoh & Basu 2008, Vázquez-Semadeni et al. 2011). In defining observational tests of star-formation theory, it is useful to retain the two extreme-case theories because the contrasts will be sharpest. Observational tests that do not unambiguously distinguish between the extreme cases may suggest that the more complex theories that include both physically important turbulence and magnetic fields may be favored.

The best and perhaps the only way to resolve the controversy about what drives the star-formation process is to observe magnetic fields and compare the results with theoretical predictions. In order to do this, I first briefly summarize theoretical models of star formation and the predictions that can be tested by observations of magnetic fields. I then describe each of the observational techniques that are available for observing magnetic fields in molecular clouds, including limitations in what can be observed and in the analysis techniques, followed by a review of the current state of the observations. After discussing all of the techniques and results, I discuss what we know based on results from all the observations. Finally, I discuss future observations that will be possible in the next few years.

2. THEORETICAL MODELS OF STAR FORMATION

2.1. Strong-Field Models

In the strong magnetic field theory, clouds are formed with subcritical masses, $M < M_\Phi = \Phi/2\pi\sqrt{G}$ (Nakano & Nakamura 1978), where M_Φ is the critical mass, Φ is the magnetic flux, and G is the gravitational constant. Hence, the magnetic pressure is sufficiently strong to counteract gravity and prevent gravitational collapse. Because the magnetic field is frozen only into the ionized gas and dust, neutral gas and dust contract gravitationally through the field and the ions, increasing mass in the cloud cores. The magnetic field strength also increases, but more slowly than does mass. This process is known as (gravity-driven) ambipolar diffusion. [Ambipolar diffusion, or breaking

of flux freezing, may also be driven on small scales by turbulence (e.g., Zweibel 1988.)] When the core mass reaches and exceeds M_Φ, the core becomes supercritical ($M > M_\Phi$), collapses, and forms stars. During the collapse, the magnetic field is dragged inward but cannot become strong enough to halt the collapse.

2.2. Weak-Field Models

The weak-field theory of star formation says molecular clouds are intermittent phenomena, with short ($\sim 10^6$ years) lifetimes. Magnetic fields are sufficiently weak that the low-density ISM is supercritical ($M > M_\Phi$). Clouds form at the intersection of turbulent supersonic flows. Generally, clouds do not become gravitationally bound, and they dissipate; those that are self-gravitating form stars in essentially a free-fall time (Elmegreen 2000). Supersonic turbulence will dissipate on roughly the free-fall timescale as collapse of gravitationally bound clouds proceeds (MacLow et al. 1998). Although magnetic pressure cannot stop the collapse, it can dominate turbulent pressure during the late stages of core collapse. An extreme version of weak-field models has the initial field so weak that the medium is super-Alfvénic as well as supercritical (Padoan et al. 2004).

Of course, the formation of clouds may lead to M/Φ varying within cloud complexes, so some volumes in a cloud complex may be subcritical and some supercritical. Hence, the subsequent evolution of different regions of a cloud complex may be best described by models with different degrees of support by magnetic fields.

2.3. Models with Significant Magnetic Fields and Turbulence

Nakamura & Li (2005) carried out simulations in a sheet approximation of molecular cloud formation and fragmentation including turbulent initial conditions and ambipolar diffusion, finding that the star-formation timescale is reduced by an order of magnitude for a subcritical cloud compared with simulations with no turbulence, but that magnetic fields nevertheless prevent most material from collapsing to form stars. Tilley & Pudritz (2007) carried out a series of decaying turbulence simulations with various initial conditions. They found that the cores that form generally have a smaller M/Φ than the original cloud, so clouds that are initially highly supercritical produce cores that are only slightly supercritical. Initially, slightly supercritical clouds collapse into sheets that fragment into cores with a different mass distribution from what is observed. Kudoh & Basu (2008) carried out 3D simulations, finding that an initial turbulent compression enhances the ambipolar diffusion and has two possible outcomes. Either M/Φ remains subcritical and the density then decreases or, for the highest density regions, ambipolar diffusion proceeds but at an enhanced rate. Vázquez-Semadeni et al. (2011) considered the formation of molecular clouds. They noted that if molecular clouds form by flows along flux tubes, for a relatively small distance along a flux tube, initially there will be little mass and M/Φ will be highly subcritical. As mass flows into the region of the cloud, M/Φ increases. They thus argue that clouds start out as atomic and subcritical and accumulate mass over $\sim$1 kpc to become molecular and supercritical as they evolve, becoming self-gravitating at about the same time. Dense cores, however, may be magnetically subcritical if they form by turbulent compression even if the cloud in which they reside is globally supercritical. Ambipolar diffusion driven by gravity may then increase the core M/Φ until the core can collapse and form stars. Their simulations ranged from slightly supercritical to slightly subcritical initial M/Φ. Subcritical clouds settle into an oscillatory regime, but eventually ambipolar diffusion leads to collapse; supercritical clouds proceed directly to star formation.

A new physics that has only recently begun to be explored for its effect on molecular cloud evolution is magnetic reconnection (Lazarian 2005). Lazarian discusses reconnection in a turbulent

medium being much faster than the larger-scale reconnection considered by the classical Sweet-Parker (Parker 1957, Sweet 1958) theory. Because this process would be most rapid in more turbulent and larger spatial-scale regions, it would lead to loss of magnetic flux early in the evolution of clouds and make it possible for subcritical clumps of the ISM to become supercritical and to gravitationally contract. This mechanism is very different from the gravity-driven ambipolar diffusion model of star formation discussed in Section 2.1. However, detailed models have not yet been presented.

2.4. Observationally Testable Theoretical Predictions

The predictions discussed in this section apply in principle to both low-mass and high-mass star-formation regions. One observational test is the magnetic field morphology. For strong fields, field lines should be smooth, both in the early stages of cloud formation and during later stages of collapse. Gravitationally bound clouds will be thin oblate spheroids because magnetic fields provide additional support perpendicular to field lines. The field lines should be parallel to the minor axes of clouds. Finally, an original morphology with parallel magnetic field lines will be transformed into an hourglass morphology because it is the tension of the bent field lines that provides support. However, the "pinch" in such hourglass morphologies should be relatively small because the strong magnetic field will severely retard collapse perpendicular to the field. In the turbulent model, during the early stage of cloud formation the magnetic field will be too weak to resist twisting by the dominant turbulence, and field lines will be chaotic. However, for gravitationally bound clouds, turbulence will dissipate as collapse proceeds and the field will become increasingly ordered. In this case, a clear hourglass field morphology will occur, with the hourglass pinch being more severe than for the strong-field model because the field will be too weak to strongly retard collapse perpendicular to the field. The strength of the pinch can be a test of the strength of the magnetic field (Basu, Ciolek & Wurster 2009).

The most direct test of the two models is provided by the very different strengths of the magnetic fields in the two theories. There are two dimensionless parameters that define the importance of magnetic fields, one with respect to kinetic energy and the other with respect to gravity. The first is the ratio of thermal to magnetic pressure, β, which parameterizes whether the gas is sub-Alfvénic or super-Alfvénic. The Alfvénic Mach number M_A may be used instead. Because nonthermal motion or turbulence is usually important in molecular clouds, the turbulent β (substituting the turbulent for the thermal speed) is also of interest. The second parameter gives the relative importance of gravity to magnetic fields; it is the mass to magnetic flux ratio, M/Φ. It is convenient to state M/Φ in units of the critical value (Section 2.1); hereinafter, M/Φ will mean the mass-to-flux ratio in units of the critical value. Obtaining M/Φ from observations is possible if the column density N and the total magnetic field strength $|\mathbf{B}|$ (hereinafter, B_{TOT}) are measured: $M/\Phi = 7.6 \times 10^{-21} N(H_2)/B_{TOT}$ (Crutcher 2004), where $N(H_2)$ is per square centimeter and B_{TOT} is in microgauss. For strong fields, clouds are initially subcritical, $M/\Phi < 1$; M/Φ must be <1 in cloud envelopes, whereas in cores ambipolar diffusion leads to $M/\Phi \approx 1$ or slightly >1. For the weak-field model, the field must be supercritical, $M/\Phi > 1$; M/Φ may take any value >1, although for the extreme-case model with very weak magnetic fields, clouds will be highly supercritical, $M/\Phi \gg 1$.

A third test is the scaling of field strength with density, which is usually parameterized as a power law, $B_{TOT} \propto \rho^{\kappa}$. Two extreme cases are compression of gas along the magnetic field, for which $\kappa = 0$ because the gas density increases but the field is unchanged, and compression perpendicular to the field, for which $\kappa = 1$ because with flux freezing both are compressed equally. In the strong-field model, as ambipolar diffusion increases M/Φ in a core, ρ increases faster than

B_{TOT}; $\kappa \leq 0.5$ is predicted (e.g., Mouschovias & Ciolek 1999). For weak magnetic fields, the magnetic field is too weak to impose a preferred direction on the collapse, in which case $\kappa \approx 2/3$ is predicted (Mestel 1966).

3. DUST POLARIZATION: OBSERVATIONAL TECHNIQUES

Interstellar dust produces thermal emission and extinction of light from background stars. Linear polarization of this radiation provides a probe of the magnetic field morphology in the ISM, including molecular clouds. This polarization requires the alignment of irregularly shaped grains. There are, however, a number of mechanisms for producing grain alignment, not all of which produce alignment with the local magnetic field. Lazarian (2007) reviewed the theory of grain alignment and concluded that the most powerful alignment mechanism is that of radiative torques. Hoang & Lazarian (2008) discussed this mechanism in detail. In this model, irregularly shaped grains differentially scatter anisotropic radiation, which spins the grains preferentially about their short axes, with precession of the spin axes being about the local magnetic field. Hence, the grain extinction cross-section is greatest perpendicular to **B**, so the maximum of the polarized light from background stars is parallel to B_{POS}, the magnetic field direction in the plane of the sky. Conversely, maximum polarized emission is perpendicular to B_{POS}. The predicted degree of polarization depends very weakly on magnetic field strength, so dust polarization does not directly give the magnitude of the magnetic field. A statistical technique for estimating the magnitude of B_{POS} from maps of linear polarization is discussed in the next section.

The required radiation field for radiative torque alignment of grains can be found in the outer regions of clouds due to radiation external to the clouds, or deep inside clouds due to radiation from protostellar and prestellar concentrations of mass in cores. Polarized starlight provides essentially infinite spatial resolution on the plane of the sky but with a coarse grid that depends on the density of background stars. It is particularly useful for probing relatively small A_V; in the case of molecular clouds this is valuable for studying large-scale magnetic field morphology within and between giant molecular cloud (GMC) complexes.

Polarized emission at millimeter and submillimeter wavelengths is useful for studying magnetic field morphologies at larger A_V corresponding to molecular clumps and cores. Polarized emission from large grains can arise even at $A_V > 20$. The degree of alignment is highly dependent on grain size, with larger grains being aligned by longer wavelength radiation. These dependences on grain size and wavelength make it possible, in principle, to both probe different regions of clouds by observing at different wavelengths and test the alignment theory by measurement of the percentage polarization at different observing wavelengths in different radiation field environments (e.g., Vaillancourt et al. 2008); but such a test would be complicated by depolarization produced by possible field tangling.

Because dust emission is generally optically thin (depending on the observing frequency), the entire line of sight is, in principle, probed in mapping polarized dust emission. The Stokes parameters Q and U give a complete description of the linear polarization; alternatively, the fractional polarization $p = \sqrt{Q^2 + U^2}/I$ (where I is the Stokes parameter I) and position angle $\theta = \frac{1}{2}\arctan(U/Q)$ are often used. Observations are usually presented as a grid of line segments to represent p and θ superposed on the total emission from a region. Although these line segments are usually referred to as polarization vectors, they are not true vectors—they have a 180° ambiguity in representing the magnetic field direction on the plane of the sky. So polarization "vectors" from different regions cannot be combined vectorially. Rather than using the nonstandard and awkward term line segments, I follow the convention and use the term vectors.

4. DUST POLARIZATION: FIELD STRENGTHS

Although polarization produced by dust does not yield direct measurements of the strengths of magnetic fields, in the early days of interstellar polarization studies Chandrasekhar & Fermi (1953) suggested that analysis of the small-scale randomness of magnetic field lines could yield estimates of the field strengths. This Chandrasekhar-Fermi (CF) method depends on the fact that turbulent motions will lead to irregular magnetic fields (because under interstellar conditions fields will be frozen into the matter). There will therefore be a perturbed or irregular component to the field that should show up as an irregular scatter in polarization position angles relative to those that would be produced by a regular magnetic field. The stronger the regular field, the more it resists being bent by turbulence. With four assumptions—that there is a mean magnetic field, that the turbulence is incompressible and isotropic, and that there is equipartition between turbulent and magnetic energy—they showed that the magnitude of the irregularity of field lines could yield the regular field strength in the plane of the sky: $B_{POS} = \sqrt{4\pi\rho}\,\delta V/\delta\phi$, where ρ is the gas density, δV is the one-dimensional velocity dispersion, and $\delta\phi$ is the dispersion in polarization position angles.

When the inferred B_{POS} is used to estimate M/Φ, it is also necessary to have a value for the relevant column density N_H. Because the CF method gives B_{POS} as a mean over an area, the mean N over the same area is used. If B_{POS} is based on observations of dust, the mean N_H is obtained from the mean extinction (for absorption) or mean emission by the dust and an assumed dust/gas ratio. Although the N_H will be uncertain, the main contribution to uncertainties in M/Φ comes from the uncertainties in the magnetic field strengths inferred from the CF method.

There are several factors that lead to errors in CF estimates of the magnetic field strength, generally overestimates. One is that polarization observations do not sample all of the structure in a tangled magnetic field along the line of sight, leading to a reduced $\delta\phi$. Ostriker, Stone & Gammie (2001) attempted to calibrate this smoothing effect by computing what the CF technique would infer for magnetic field strengths if their simulations of interstellar clouds (with, of course, known **B**) were "observed." They found that the B_{POS} inferred from the CF formula would yield reliable results so long as the field strengths were relatively strong ($\delta\phi < 25°$) if a correction factor of $\approx$0.5 were applied, a value that has been used by many observers. Heitsch et al. (2001) extended this type of numerical study to include the effects of limited telescope resolution (which spatially smooths polarization maps) and self-gravity (which was not originally considered). They found that self-gravity had little effect on the results and suggested a modification to the CF formula that would improve the accuracy for weak fields. Falceta-Gonçalves, Lazarian & Kowal (2008) found that calculation of the two-point correlation function of the polarization position angles for their simulations of interstellar clouds would make it possible to obtain estimates of B_{POS} that differed by less than 20% from actual values in the simulations.

One problem in applying the CF method is that there may be ordered structure in B_{POS} that is not due to turbulence. The straightforward calculation of $\delta\phi$ ignoring this structure would overestimate the turbulence contribution and, hence, underestimate the magnetic field strength. A method of dealing with this is to fit an assumed smooth pattern (such as an hourglass) to the polarization data and then calculate $\delta\phi$ after subtracting the pattern from the measured polarization position angles. Hildebrand et al. (2009) proposed a method, similar to that of Falceta-Gonçalves, Lazarian & Kowal (2008), for finding the turbulent contribution to $\delta\phi$ that does not require the assumption of a particular pattern. One computes the two-point correlation of the observed position angles, which they call the angular dispersion function. With the assumption that the magnetic field is composed of a large-scale structured field and a turbulent field that are statistically independent, they note that the contribution of the structured component to the angular

dispersion function will increase approximately linearly for small separations, whereas the turbulent component contribution will be approximately constant at separations exceeding the turbulence correlation length. This different behavior of the two components allows them to separate out the turbulent component and compute the $\delta\phi$ required by the CF method. It also gives the ratio of the turbulent to the ordered magnetic field. A possible problem with this technique is that, especially with limited observational data, the largest-scale turbulent eddies may be interpreted as a large-scale structured field, so the $\delta\phi$ would be underestimated and, thus, B_{POS} overestimated.

Houde et al. (2009) proposed further refinements to this method; they put the CF method on a formal analytic basis by including the effects of a large-scale structured field and a turbulent field, explicitly including integration over the telescope beam and along the line of sight of both the magnetic field structure and the polarized emission structure (which can be due purely to density structure and not turbulence). This therefore accounts for the aforementioned problem of smoothing of structure, leading to a reduced $\delta\phi$. To do this they assumed stationarity, homogeneity, and isotropy in the magnetic field strength as well as statistical independence between its large-scale structured and turbulent components. In order to proceed to analyze real data, information about the telescope beam profile and the autocorrelations of magnetic field and polarization emission is needed; they assumed that these have Gaussian form. The correlation length scales for the turbulent magnetic field and for the polarized emission specify the width of these Gaussians; they are assumed to be much smaller than the thickness of the cloud being observed, so there are many turbulent and polarized emission cells along the line of sight. With simplifications such as assuming that the turbulent polarized emission can be neglected, they derived an expression that makes it possible to find the magnitudes of the regular and turbulent magnetic fields, the turbulent correlation length scale (closely related to the turbulent ambipolar diffusion scale), and the turbulent power spectrum from linear polarization maps.

There remain significant uncertainties in applying the CF method, however. To what extent the Houde et al. (2009) assumptions of stationarity, homogeneity, and isotropy affect the results is unclear. Molecular clouds are clearly not homogeneous and isotropic, and gradients in magnetohydrodynamic (MHD) turbulent velocities tend to be smaller in the direction of the magnetic field (Goldreich & Sridhar1995). Because one can only determine the line-of-sight turbulence through observing nonthermal line widths, the value used for δV may be incorrect. Further, one must choose a spectral line that one believes samples the same regime as the polarized emission and use an estimate for the gas density for the regions of polarized emission. Because grain alignment seems to be suppressed at high optical depths, just what regions of clouds are sampled by polarized emission is unclear. For all these reasons, B_{POS} obtained even with the most sophisticated analysis techniques with the highest quality data remain uncertain by a factor of about two or more.

A new method was recently proposed by Koch, Tang & Ho (2012), which assumes that a change in dust emission intensity is a measure of the resulting direction of motion in the MHD force equation. The method leads to maps of the magnetic field strength where both polarized and total dust emission can be mapped.

5. DUST POLARIZATION: OBSERVATIONAL RESULTS

5.1. Background Stars

The interstellar magnetic field was first detected by Hiltner (1949) during an attempt to detect polarization due to scattering by electrons in atmospheres of early-type stars. Heiles (2000) compiled a catalog of polarization observations toward 9286 stars by agglomerating previous catalogs. Further observations during the past decade have extended the list to many additional stars. Such

observations probe magnetic field morphology in the outer parts of molecular clouds, where the extinction is not so high, and make it possible to study the regularity of the field and how it is oriented with respect to the morphologies of clouds. Goodman et al. (1990) summarized these results and added observations near molecular clouds in Taurus, Ophiuchus, and Perseus.

Although the starlight polarization patterns around dark clouds were generally fairly smooth, no universal orientation of magnetic fields probed by background starlight polarization has been found, with B_{POS} sometimes approximately parallel and sometimes perpendicular to clouds' major axes and sometimes intermediate. Moreover, the polarization patterns did not seem to change in the vicinity of high-density concentrations in dark clouds, suggesting that the optical polarimetry did not sample magnetic fields in the molecular gas. In order to better explore denser and more highly extinct regions, Goodman et al. (1995) carried out near-IR polarization observations through the dark cloud L1755, sampling extinctions up to $A_V \approx 10$ mag. They found that the near-IR polarization pattern was very similar to the pattern observed at optical wavelengths that sampled lower A_V and that the percentage polarization did not increase with extinction, suggesting that the dust in the dark cloud was not contributing to the near-IR polarization.

However, others have found that near-IR polarization does increase with extinction. **Figure 1** shows optical and near-IR starlight polarization vectors superposed on a ^{13}CO map of the Taurus dark-cloud complex (Chapman et al. 2011). They found that the near-IR

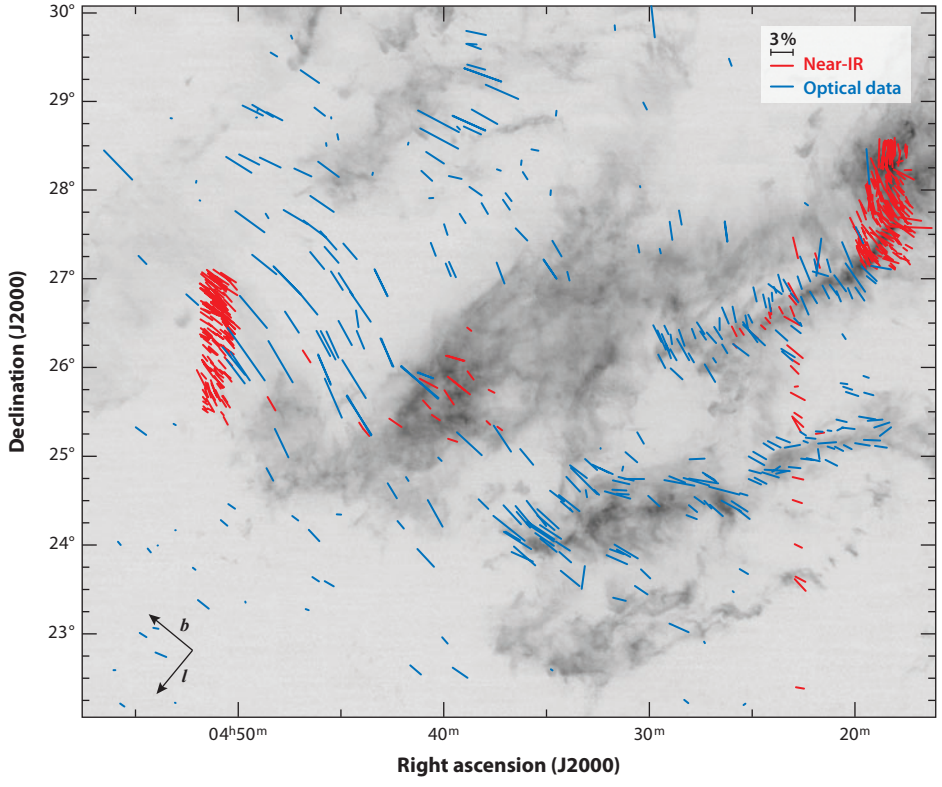

Figure 1

Magnetic field morphology in the Taurus dark-cloud complex superposed on a ^{13}CO map (Chapman et al. 2011). Blue lines show polarization measured at optical wavelengths and red lines show near-IR (H-band and I-band) polarization.

polarization increased with column density up to $A_V \sim 9$ mag, the limit of their data. The magnetic field has a generally smooth structure, although its direction is not the same throughout the complex. Toward the northern part of L1495, the polarization vectors (and the magnetic field) are primarily along the filament. To the south as the filament turns to the east, becoming B213, the magnetic field becomes perpendicular to the long axis of the filament. The magnetic field is primarily parallel to the long axis of L1506, whereas it is neither clearly parallel nor perpendicular to the B18 clumpy filament. This region shows the diversity of alignments of B_{POS} with molecular filaments. Chapman et al. used the CF technique to estimate B_{POS} in nine subregions, finding that $B_{POS} \sim 10$ μG in low-density regions, ∼25 μG in the B213/Filament/L1495 subregion, and ∼42 μG in the Heiles Cloud 2 region. They noted that OH Zeeman measurements toward 11 cores in Taurus (Troland & Crutcher 2008) gave significantly smaller results for B_{LOS}, suggesting that **B** in Taurus is primarily in the plane of the sky. If one assumes that $B_{POS} \approx B_{TOT}$, M/Φ is subcritical by ∼2; they argued that the Taurus complex is magnetically supported on a ∼2 pc scale. However, uncertainties in the CF method (Section 4) may overestimate magnetic field strengths by at least a factor of 2, so the Taurus molecular cloud complex is not unambiguously subcritical.

5.2. Dust Emission

Of course, in addition to attenuating starlight, interstellar grains emit thermal radiation. The first attempt to detect linearly polarized dust emission in the far-IR (Dennison et al. 1977) was unsuccessful; the first success (Cudlip et al. 1982) was achieved toward M42. Polarimetry of dust emission toward molecular clouds then fairly rapidly became a standard observational tool, with Hildebrand's group (e.g., Hildebrand, Dragovan & Novak 1984) producing increasingly sensitive and extensive maps of magnetic field morphologies in the plane of the sky toward molecular clouds. Dotson et al. (2010) presented an archive of data obtained with the Hertz polarimeter used at the Caltech Submillimeter Observatory (CSO), which contains over 4,300 polarization measurements at 350 μm in 56 Galactic objects and 2 galaxies, together with polarization maps and tabulated results. Curran & Chrysostomou (2007) presented and discussed polarization maps obtained with the Submillimetre Common-User Bolometer Array (SCUBA) array on the James Clerk Maxwell Telescope (JCMT) at 850 μm, with data for 16 high-mass star-formation regions. They found that there is a variety of magnetic field morphologies with some very ordered fields, suggesting that the field is strong enough to resist twisting by turbulence. Using the CF method, they inferred B_{POS} (probably overestimated, see Section 4) toward 14 cores, finding that B_{POS} ranged from <0.1 to 5.7 mG, with the majority in the 0.2–0.4-mG range. They found no relation between mean field direction and outflow direction for the whole sample, although some alignments were found. Of the three objects with the strongest field strengths, DR21(OH)N and RCrA have the field direction perpendicular to the projected major axis of the dust emission, consistent with magnetic support, whereas Cep A has the field parallel to its major axis. Matthews et al. (2009) rereduced all of the SCUBA JCMT polarization data and presented the results in an archive; the 83 regions with significant detections consisted of 48 star-forming regions, 11 young stellar objects, 9 Bok globules, and 6 starless or prestellar cores.

Tassis et al. (2009) carried out a statistical analysis to infer the intrinsic shapes and magnetic field orientations of 24 clouds for which Hertz polarimeter data were available. They found the best fit to be for oblate disks with the intrinsic magnetic fields oriented close (∼24°) to the minor axes. However, due to the small number of clouds, they were unable to reject alternative configurations.

Li et al. (2006) studied whether the magnetic field direction in molecular clouds was correlated with the Galactic plane. They mapped four GMCs in the Galactic disk with the SPARO 450-μm polarimeter on a 2-m telescope at the South Pole. They found a statistically significant correlation

of the magnetic field directions with the Galactic plane and argued that the field direction is preserved during the formation of the molecular cloud complexes. By comparing the dispersion in observed polarization vectors with those in Ostriker, Stone & Gammie (2001) simulations, they concluded that the magnetic and turbulent energies are comparable. Novak, Dotson & Li (2009) revisited such a comparison with higher resolution Hertz polarimeter observations. They found that agreement between observations and simulations is best when the total magnetic energy is at least as large as the turbulent kinetic energy.

The eight inserts in **Figure 2** show examples of dust emission polarization of molecular cores in Orion; the observed polarized emission vectors have been rotated by 90° so the direction of the magnetic field is shown. In general, the field morphology is fairly smooth and usually perpendicular

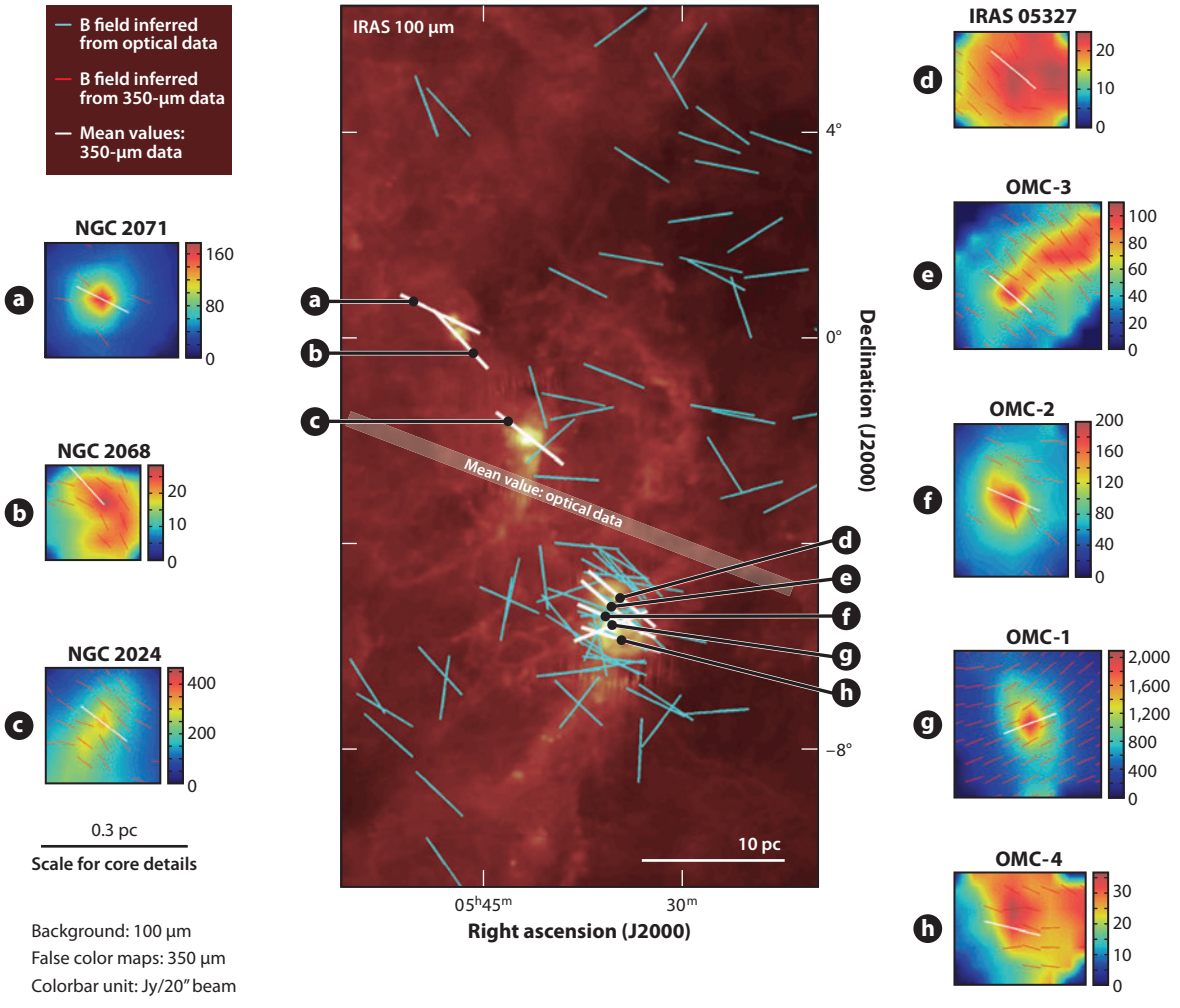

Figure 2

Magnetic field morphology in the Orion molecular cloud region (Li et al. 2009). Light blue lines show optical data that sample the lower A_V regions, and red lines show 350-μm Hertz Caltech Submillimeter Observatory data that sample the polarization of dust emission in each of the cores (A–H). The mean B_{POS} directions over the extended region and in each core are shown by thick white lines. Background shows the IRAS 100-μm image.

to the projected major axis of the cores (NGC 2024, OMC3, OMC1), where significant noncircular cores are observed. This is the field morphology predicted for gravitational contraction mainly along magnetic field lines. Toward NGC 2024 there is some evidence of the hourglass field morphology. However, the NGC 2068 field is along the "kidney" shaped core, which may be two cores. The purpose of this figure is to compare the magnetic field morphology in cores within the Orion Molecular Cloud with the field morphology in the more diffuse gas in which the cores are embedded. Li et al. (2009) conclude that the mean magnetic field direction in the cores (except for OMC1) are well aligned with each other and with the mean field direction traced by optical starlight polarization in the more diffuse gas. They find that the Orion result is not unique; for 25 cores in their sample, there is a significant correlation between the field direction in the cores and in the surrounding more diffuse gas. Comparison of this observational result with results obtained from simulations of molecular clouds (Ostriker, Stone & Gammie 2001) lead to the conclusion that a globally super-Alfvénic cloud cannot reproduce the observational result.

However, Padoan et al. (2004) compared the column density power spectra inferred from ^{13}CO $J = 1$–0 maps of the Perseus, Taurus, and Rosetta molecular cloud complexes with power spectra obtained from their simulations of molecular cloud formation and evolution. They found that the observed power-law index was essentially the same in the three molecular cloud complexes, 2.75. For simulations with Alfvénic flow velocities, they found a power-law index of 2.25, whereas for a highly super-Alfvénic flow they found 2.71. They found that the approximately equilibrium model was ruled out at a confidence level exceeding 99%. Hence, they concluded that the average magnetic field strength in molecular clouds may be much smaller than required for support against gravity.

Interferometer array maps of the polarization of dust emission explore the magnetic field at higher resolution than the single-dish results. The Berkeley-Illinois-Maryland Array (BIMA) produced the first such results for Orion-KL (Rao et al. 1998), NGC 1333 IRAS4A (Girart, Crutcher & Rao 1999), W51 (Lai et al. 2001), NGC 2024 (Lai et al. 2002), and DR21(OH) (Lai, Girart & Crutcher 2003). In general, these maps show fairly regular polarization structure that is consistent with that seen toward these clouds with single-dish polarimetry, although there are small-scale regions where the polarization vectors are at significantly different angles from the mean. The CF method gave field strengths $B_{POS} \sim 1$ mG (probably overestimated, see Section 4) with the regular field generally dominating the turbulent field. Toward NGC 2024 and NGC 1333 IRAS4A, evidence for hourglass morphology fields was found.

The Submillimeter Array (SMA) continued mapping of dust polarization of molecular clouds; because it can observe at a higher frequency (~350 GHz) than could BIMA, the higher emissivity of dust at the higher frequency allows the SMA to achieve greater sensitivity than did BIMA. **Figure 3** shows SMA observations of the low-mass (~1.2 $M_\odot$) protostellar system NGC 1333 IRAS4A. On the left is the map made with relatively short interferometer baselines (Girart, Rao & Marrone 2006), so most of the more extended structure is detected. The magnetic field shows a clear hourglass morphology, confirming the BIMA result. This morphology is expected for gravitational contraction and flux freezing. Contraction is preferentially along the magnetic field, but contraction perpendicular to the field pulls field lines in, forming the hourglass shape. Such an hourglass morphology does not imply ambipolar-diffusion-driven contraction, only that the field strength is sufficiently strong to dominate turbulence. They fitted parabolas to the observed field lines in order to subtract out the contribution of the regular field of the hourglass to the dispersion of the observed magnetic vectors. Then the CF method gives $B_{POS} \approx 5.0$ mG (probably overestimated, see Section 4), which gives $M/\Phi \approx 1.7$ times critical, which is slightly supercritical. They also found $\beta_{turb} \approx 0.02$, so the magnetic energy significantly dominates the turbulent energy.

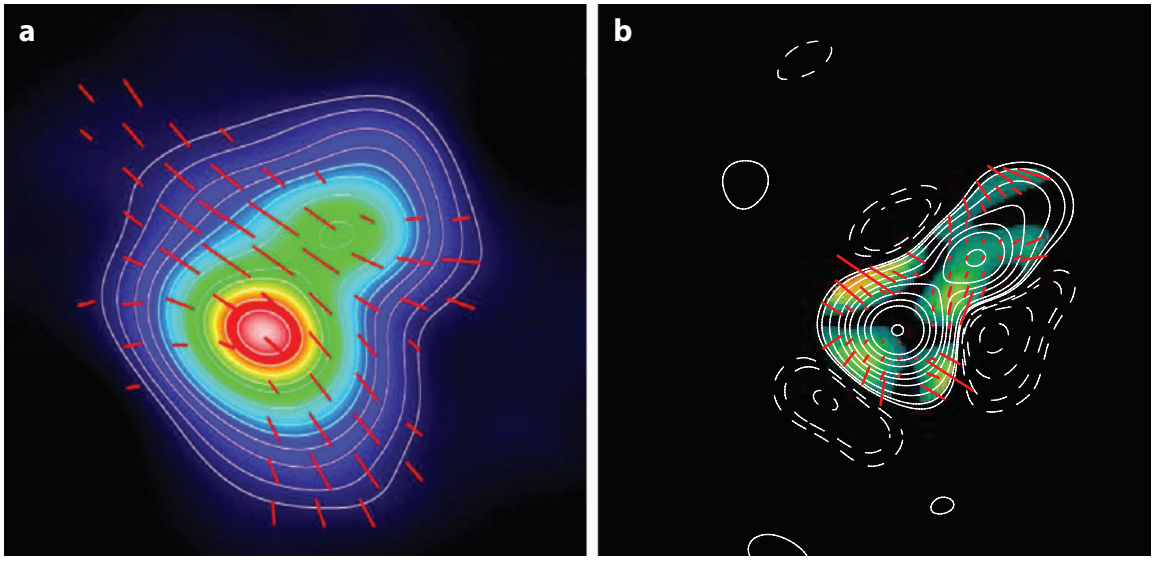

Figure 3

(*a*) NGC 1333 IRAS4A magnetic field with short Submillimeter Array (SMA) baselines (Girart, Rao & Marrone 2006). Dust emission flux is shown as white contours and color, whereas the red vectors show the magnetic field in the plane of the sky. (*b*) NGC 1333 IRAS4A magnetic field with only long SMA baselines (S-P Lai, unpublished), which is sensitive only to small-scale structure. White contours show dust emission flux, colors show polarized flux, and red vectors show the magnetic field in the plane of the sky. The negative flux contours are due to the missing flux that is filtered out by the interferometer. The separation of the two intensity peaks is ∼400 AU.

S-P Lai (unpublished information) has observed NGC1333 IRAS4A with the longest baselines of the SMA. A map that excludes the shorter baselines is shown in **Figure 3*b***; without the short baselines, larger-scale spatial structure is filtered out. The inner parts of the hourglass morphology are detected, but in addition, the magnetic field is orthogonal to the axis of the hourglass to the southeast and northwest. This is interpreted as a toroidal magnetic field due to rotation of a protoplanetary disk in the inner parts of the system.

On larger spatial scales (10 arcsec), Attard et al. (2009) mapped the dust continuum polarization at 350 μm with the SHARP polarimeter on the CSO single dish; they found that the polarization pattern was fairly uniform with the magnetic field aligned along the hourglass axis seen with the SMA. Thus, the hourglass pinch is indeed a pinch in a larger-scale uniform magnetic field. They also mapped HCN $J = 4$–3 emission and found inverse P Cygni profiles, indicating collapse velocities of 0.64 km s^{-1} over an area about four times larger than the magnetic pinch and an age of the infalling envelope of $\sim 2 \times 10^5$ year. Their CF analysis yielded $B_{POS} \approx 1.4$ mG in the extended envelope and $M/\Phi \approx 0.44$ or subcritical, which is inconsistent with the observed infall. This is perhaps indicative of the uncertainties in results based on the CF method.

Houde et al. (2009) applied their more sophisticated CF technique (Section 4) to SHARP CSO data for OMC1. They found $B_{POS} \approx 760$ μG, which is comparable to the $B_{LOS} \approx 360$ μG from a CN Zeeman observation (Crutcher et al. 1999), and commented that the result with the original CF technique would be $B_{POS} \approx 3.5$ mG. They further found that the ratio of the turbulent to regular magnetic field was about 0.5 and that the turbulent correlation length $\delta \approx 16$ mpc. This δ should be closely related to the scale on which the ionized and neutral components of the gas decouple due to turbulent ambipolar diffusion. This scale was determined to be 10 mpc by Houde et al. (2011) from a SMA polarization map of Orion KL. They also analyzed the Girart, Rao &

Marrone (2006) map of NGC1333 IRAS4A (**Figure 3**) to obtain a tentative scale value of 2.2 mpc (450 AU).

In summary, maps of the polarization produced by dust in molecular clouds are generally fairly smooth, suggesting that magnetic fields are sufficiently strong to resist twisting by turbulence. Molecular cores generally have similar field directions to those in the GMCs in which they reside. High angular-resolution maps of cores occasionally show hourglass morphology fields that would be produced by gravitational contraction, but not necessarily driven by ambipolar diffusion. The statistical CF method, including recent refinements, gives estimates for magnetic field strengths, but uncertainties are likely a factor of at least two.

6. ZEEMAN EFFECT: OBSERVATIONAL TECHNIQUES

The Zeeman effect is the only available technique for directly measuring magnetic field strengths in interstellar clouds (e.g., Crutcher et al. 1993). Zeeman splitting is proportional to a factor Z that is dependent on the specific spectral transition. The strongest Zs are approximately equal to the Bohr magneton, $eh/4\pi mc = 1.40$ Hz/μG, which occur for species with an unpaired electron (paramagnetic species). Because Z does not depend on spectral-line frequency, for a given Zeeman splitting (in Hertz), sensitivity to the Zeeman effect decreases with increasing spectral-line frequency. Unfortunately, most of the common interstellar molecules have all their electrons paired (nonparamagnetic species) and therefore do not have strong Z factors. To date, the Zeeman effect has been detected unambiguously in nonmasing interstellar gas only in HI, OH, and CN lines; other promising species are C_2H, SO, C_2S, C_4H, CH, and C^+ recombination lines. Zeeman splitting has been detected in OH, CH_3 OH, SiO, and H_2O masers.

In the normal Zeeman effect, a spectral line is split into three components, with a π component unshifted in frequency and two σ components shifted by $\Delta\nu_Z = \pm Z|\mathbf{B}|$, where Z is a Zeeman coefficient that depends on the spectral transition. The strength of the linearly polarized π component is proportional to the strength of the magnetic field in the plane of the sky parallel to **B**. The σ components are generally elliptically polarized. The elliptical polarization is a combination of linear polarization perpendicular to **B** in the plane of the sky and circular polarization proportional to the strength of the magnetic field along the line of sight. The sense of the circular polarization of the two σ components reverses with B_{LOS} toward or away from us. From $\Delta\nu_Z$, the degree of elliptical polarization of the σ components, and the relative amplitudes of the σ and π components, it is possible, in principle, to infer full information about **B** (Crutcher et al. 1993).

However, for all Zeeman detections except OH masers, the Zeeman splitting $\Delta\nu_Z \ll \delta\nu$, where $\delta\nu$ is the spectral-line width. In such cases, one only obtains information about the line-of-sight component B_{LOS} of **B**; the Stokes V spectrum has the shape of the first derivative of the Stokes I spectrum and is proportional to $(\Delta\nu_Z/\delta\nu) \times B_{LOS}$. Standard practice is to fit $dI/d\nu$ to the observed V spectrum, with B_{LOS} being the free parameter determined by the strength of the V spectrum. One also finds the direction of B_{LOS} from the sign of the fit of $dI/d\nu$ to Stokes V; the convention is that a positive sign means the magnetic field is pointed away from the observer. Information about B_{POS} would come from the Stokes Q and U spectra, with strengths proportional to $(\Delta\nu_Z/\delta\nu)^2 \times B_{POS}$. For $\Delta\nu_Z \ll \delta\nu$, the Stokes Q and U Zeeman signals are too weak to detect, except for strong maser lines. Hence, Zeeman observations (except for OH masers) reveal only the magnitude and direction (toward or away from us) of B_{LOS}.

Structure in **B** either along the line of sight or within the telescope beam can reduce the measured effect. However, such information loss may be avoided if regions with different B_{LOS} produce spectral lines with different radial velocities and/or line widths. The procedure would be

to fit for the multiple line components in the Stokes I spectrum and then fit the Stokes V spectrum for multiple B_{LOS} in each of the line components.

With only one component of the magnetic vector **B** measurable, the Zeeman effect gives directly only a lower limit to the total magnetic field strength. Because a Zeeman measurement gives only a lower limit to B_{TOT} for an individual cloud, it is necessary to resort to statistical studies of a large population of clouds to infer astrophysically meaningful information (e.g., Heiles & Crutcher 2005). Most of the earlier Zeeman studies implicitly assumed that all clouds in their sample have $|B_{TOT}| = B_0$, with B_0 being a Delta function. This implies that the measured B_{LOS} be uniformly distributed between $-B_0$ and B_0; then the median and mean of the set of measured $|B_{LOS}| = \frac{1}{2}B_0$. Hence, one simply determines the mean of $|B_{LOS}|$ to infer B_0. Because M/Φ is often the desired quantity, an extension of this approach is to divide the directly observed M/Φ by three, which is the mean correction for a randomly oriented set of uniform plane-parallel clouds with **B** parallel to the minor axis (Heiles & Crutcher 2005). However, the approaches that deal only with mean or median values ignore the possibly large variation in B_{TOT} in the sample. A more sophisticated analysis is possible that can provide information about the range in B_{TOT}. Basically, one measures the probability distribution function (PDF) of B_{LOS}, $P(B_{LOS})$, over a sample of clouds, with the goal of inferring the PDF of the total magnitude of **B**, $P(B_{TOT})$. An application of this approach is discussed in detail below.

7. ZEEMAN EFFECT: OBSERVATIONAL RESULTS

7.1. Extended (Nonmaser) Regions

Intensive searches for the Zeeman effect in the ISM went on for several years before the first detection was achieved, in 21-cm absorption lines of HI toward the Cassiopeia A supernovae remnant (Verschuur 1968). His subsequent work achieved only three additional detections over the next five years, toward Orion A, M17, and Taurus A. This early history shows the difficulty of interstellar Zeeman observations, both because of the weakness of the effect and the problems of controlling instrumental polarization effects. Of these four detections, three were in the HI associated with molecular clouds; only the Taurus A line-of-sight samples the diffuse, atomic ISM. Attempts to detect the Zeeman effect in molecular lines in order to observe more directly magnetic fields in molecular clouds also met with initial failure (Crutcher et al. 1975) due to the weakness of OH emission lines. The first success was of OH absorption toward the NGC 2024 molecular cloud (Crutcher & Kazès 1983). The list of detected Zeeman species was extended to CN (Crutcher et al. 1999), but attempts to detect the Zeeman effect in other species have not as yet resulted in definite detections.

The three species with Zeeman detections (excluding masers) do make it possible to measure B_{LOS} over the wide range of densities in the ISM from diffuse HI clouds to molecular cores. HI in emission samples both the warm neutral and the cold neutral diffuse medium, with densities ranging roughly from 1 to 100 cm^{-3}. HI in absorption toward molecular clouds can sample densities of $\sim 10^2$–10^4 cm^{-3}, about the same densities that the ground-state 18-cm lines of OH sample. Finally, with a critical density of $\sim 10^5$ cm^{-3}, the 3-mm lines of CN in emission sample densities of $\sim 10^5$–10^6 cm^{-3}.

Because a major goal of magnetic field measurements is to test predictions of star-formation theory, it is necessary to estimate the N_H and/or n_H probed by the Zeeman transition that is observed. N_H is usually well known for HI, for which both the line optical depth and the spin temperature may be determined by observing the line in absorption toward a continuum source and in emission at nearby positions (e.g., Heiles & Troland 2003). Usually the H_2 fraction is

very small for these lines of sight, so $N_{HI} \approx N_H$. Except in very special cases, inference of n_H is by assuming a standard value for the interstellar pressure in the HI regions and finding n_H from the spin temperature (e.g., Crutcher et al. 2010). For OH, finding N_{OH} from the Stokes I data is generally straightforward (e.g., Crutcher 1979). N_H then depends on a calibration of [OH/H] by Crutcher (1979) based both on measurement of N_{OH} from optical interstellar lines toward stars of known A_V and on estimates of A_V from star counts. Estimates of n_H for OH studies generally come from mapping the extent of OH on the sky and dividing N_H by the mean diameter. In a few cases, n_H is assumed to be a mean value obtained for other clouds. The situation for CN is probably the least certain (e.g., Falgarone et al. 2008). Falgarone and colleagues took n_H from literature studies of CS lines; CS and CN have similar critical densities. They found that the ratios of hyperfine CN lines were consistent with being optically thin with approximately thermal excitation; N_{CN} then followed from an assumed excitation temperature of CN based on kinetic temperatures found from other studies. N_H then depends on an assumed [CN/H] based on studies by Turner & Gammon (1975) and Johnstone, Boonman & van Dishoeck (2003). The consistency of these results was checked by mapping the CN distribution, with the assumption that the line-of-sight thickness of a cloud equaled the mean diameter on the plane of the sky. Statistical techniques for estimating B_{TOT} from the measured B_{LOS} contribute significantly to uncertainties in the inferred M/Φ, as discussed below. Just how much uncertainties in N_H and n_H contribute to uncertainties in M/Φ and κ (in the $B \propto n^{\kappa}$ relation) is difficult to determine. Because these parameters are inferred statistically from the entire data set, uncertainties in the individual clouds are less important than if there is a systematic error. Given the uncertainties introduced by being able to observe only B_{LOS}, uncertainties in N_H or n_H seem unlikely to dominate uncertainties in the inferred M/Φ and κ.

Crutcher (1999) summarized the state of Zeeman observations in molecular clouds and discussed the results. At that time there were 27 sensitive Zeeman measurements and 15 detections. That analysis found the following results for the molecular clouds studied. (*a*) Internal motions are supersonic but approximately equal to the Alfvén speed. (*b*) The ratio of thermal to magnetic pressures is $\beta_p \approx 0.04$, implying that magnetic fields are important in the physics of molecular clouds. (*c*) The mass-to-magnetic flux ratio M/Φ is about twice critical, which suggests that static magnetic fields alone are insufficient to support clouds against gravity. (*d*) Kinetic and magnetic energies are approximately equal, which suggests that turbulent and larger-scale regular magnetic fields are roughly equally important in cloud energetics. (*e*) Magnetic field strengths scale with gas densities as $B_{TOT} \propto \rho^{\kappa}$ with $\kappa \approx 0.47$; this agrees with the prediction of ambipolar-diffusion-driven star formation. However, these conclusions were based only on the 15 detections of the Zeeman effect in molecular clouds with widely varying properties, from dark clouds that are sites of low-mass star formation to dense molecular clouds associated with recently formed OB stars. The nondetections were ignored, a clear statistical bias.

Bourke et al. (2001) carried out an OH Zeeman survey, primarily in the Southern Hemisphere, of 23 additional molecular clouds. They achieved one definite and one probable new detection and set significant limits on B_{LOS} for the others. They combined these data with those discussed by Crutcher (1999) and two additional clouds observed by others (including both detections and nondetections) to analyze the role of magnetic fields. They found that the set of clouds was consistent with having a magnetically supercritical M/Φ, in agreement with Crutcher (1999), but also argued that averaging of the Zeeman effect over the telescope beam could play a significant role in reducing the B_{LOS} that were observed.

The next major Zeeman survey was carried out in OH lines toward dark clouds (Troland & Crutcher 2008). They observed 34 positions and obtained 9 detections. They analyzed both detection and nondetection results to infer mean values of astrophysical quantities, finding that M/Φ is supercritical by $\sim$2 and that the mean Alfvénic Mach number $M_A \sim 2$. The small beam

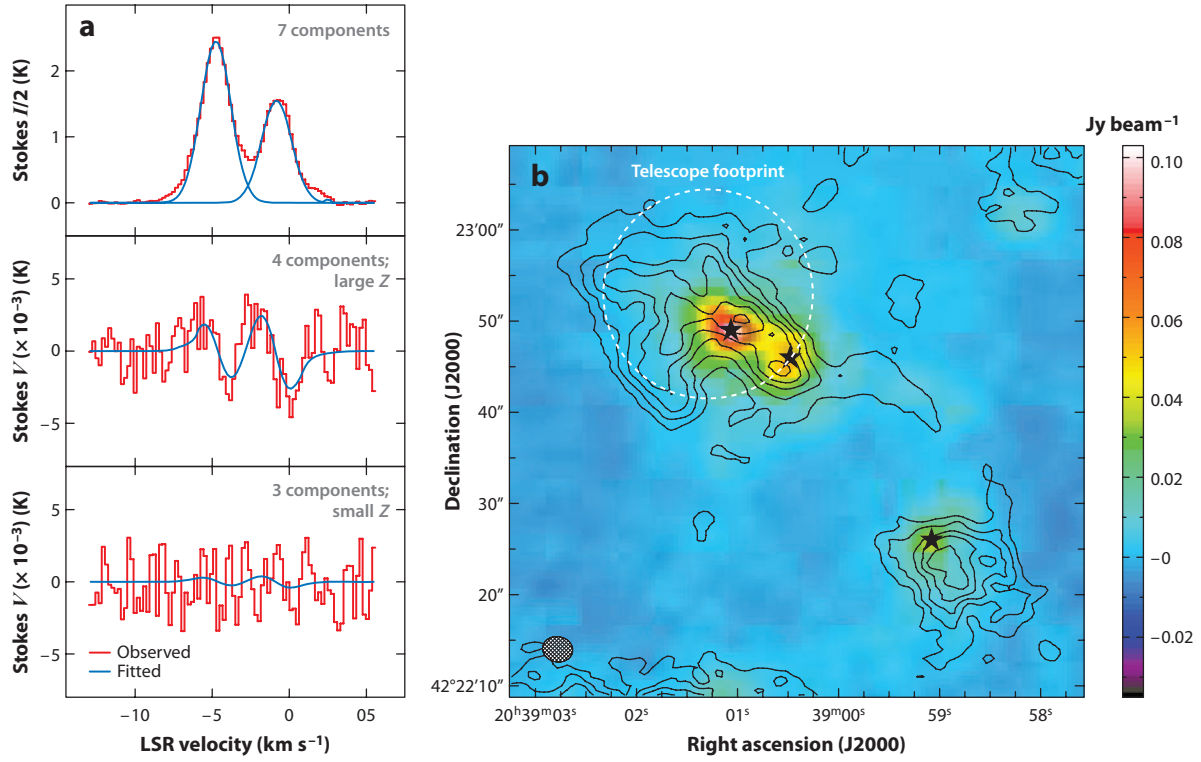

Figure 4

(*a*) CN Zeeman Stokes *I* and *V* profiles toward DR21(OH) (Crutcher et al. 1999). The two velocity components were fitted simultaneously for the seven hyperfine CN lines to derive the independent B_{LOS} for each velocity component. Because the hyperfine components have different Zeeman coefficients *Z*, this procedure separates Zeeman splitting from instrumental effects. The middle panel shows the observed and fitted Zeeman spectra for the four hyperfine components with large *Z*, whereas the bottom panel shows the fit for the three hyperfine components with small *Z*. (*b*) CARMA map of velocity-integrated CN toward DR21(OH) (N. Hakobian, R.M. Crutcher, in preparation). Contours are CN, color is dust continuum emission, and the dotted circle is the footprint of the CN Zeeman IRAM 30-m telescope beam. The CN velocity component at $V_{LSR} \approx -5$ km s^{-1} is strongest in the DR21(OH) MM1, MM2 region (*stars*) in the northeast, where the strongest dust emission is found. Although the $V_{LSR} \approx -1$ km s^{-1} velocity component peaks ~40 arcsec southwest of the 30-m telescope pointing position near the DR21(OH)W dust peak (*star*), it is widely distributed and has about half the strength of the -5 km s^{-1} component within the IRAM 30-m beam. About 50% of the single-dish CN flux is detected by CARMA, suggesting that interferometric Zeeman mapping is possible. Abbreviation: LSR, local standard of rest.

of the Arecibo telescope (3 arcmin) that was used reduced the possible effects of beam averaging that might be important for results obtained with smaller telescopes, and the analysis used all observations rather than just detections.

Finally, Falgarone et al. (2008) carried out a CN Zeeman survey of dense molecular cores. **Figure 4** shows an example of the data. Together with earlier CN Zeeman observations (Crutcher et al. 1996, 1999), there were 14 positions observed with significant sensitivity and 8 CN Zeeman detections. The analysis techniques were similar to that of the OH dark cloud survey (Troland & Crutcher 2008). The mean M/Φ was supercritical by ~3 and $M_A \sim 1.5$.

7.2. Analysis

In spite of a range of molecular cloud physical conditions and types being observed, the results of all of the Zeeman studies described above are very similar: (*a*) the *mean* mass-to-flux ratio M/Φ

is supercritical by a factor of ∼2–3, which means that the magnetic field is not able to support the molecular clouds against gravitational collapse, and (*b*) the mean Alfvénic Mach number M_A is ∼2, which means that kinetic energy (dominated by turbulence rather than thermal motions in these clouds) is slightly stronger than magnetic energy. However, one should keep in mind that systematic uncertainties in the $N(H_2)$ and $n(H_2)$ are probably ∼2, so these mean results are consistent with molecular clouds being magnetically critical (magnetic field balancing gravity) and in equilibrium between kinetic and magnetic energies, or with the magnetic fields being too weak by ∼4 in the mean for these equipartition conditions.

The emphasis on mean values in the last paragraph is due to the fact that only a lower limit to B_{TOT} is available directly from interstellar Zeeman measurements because only one of the three components of the vector **B** can be measured. However, it is possible to obtain information about the distribution of B_{TOT} values. The key lies in inferring the PDF of the total field strength, $P(B_{TOT})$, from the observed PDF of the observed line-of-sight component, $P(B_{LOS})$. In this analysis, a single B_{TOT} is assigned to each cloud and refers to the total field strength averaged over the area covered by the observation of B_{LOS} toward each cloud. The assumption of this type of analysis is that the observed sample is sufficiently large and diverse that the angles θ between the lines of sight and **B** are randomly distributed; for each line of sight, $B_{LOS} = B_{TOT} \cos\theta$. Then, from an assumed $P(B_{TOT})$ one can compute $P(B_{LOS})$. By comparing the computed $P(B_{LOS})$ with the observed $P(B_{LOS})$, one can assess the probabilities that each of the assumed $P(B_{TOT})$ represent the observed Zeeman data. This approach was first employed by Heiles & Troland (2005) for HI Zeeman observations of diffuse atomic clouds; they found that their HI data were insufficient to provide strong constraints on $P(B_{TOT})$.

Figure 5 shows two examples of the PDFs. If all the B_{TOT} in a sample of clouds were the same, then the PDF of $B_{LOS} = B_{TOT} \cos\theta$ would be flat, i.e., the observed $|B_{LOS}|$ would be equally distributed between 0 and B_{TOT}. In this case, $|\bar{B}_{LOS}| = \frac{1}{2} B_{TOT}$, so one obtains the total field strength simply by finding the mean of all the observed $|B_{LOS}|$ and multiplying by 2. For many other "reasonable" $P(B_{TOT})$, $|\bar{B}_{LOS}| \approx \frac{1}{2}\overline{B}_{TOT}$ (Heiles & Crutcher 2005). The mean values of M/Φ and M_A discussed above for various Zeeman surveys were obtained using this simple assumption. But this simple analysis of the Zeeman data tells us nothing about the distribution of the B_{TOT} in the sample of clouds observed. **Figure 5** also shows $P(B_{TOT})$ and the corresponding $P(|B_{LOS}|)$ if the B_{TOT} in the sample of clouds were uniformly distributed between 0 and some maximum

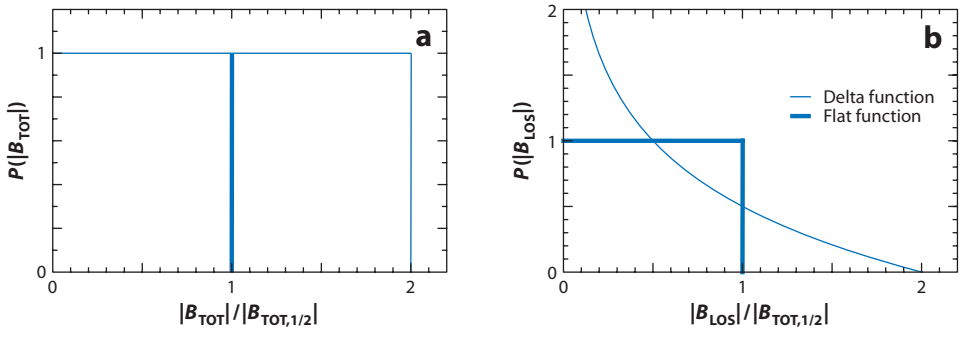

Figure 5

Plots of the two probability distribution functions (PDFs) for (*a*) the total field strengths and (*b*) the associated PDFs for the observed line-of-sight field strengths. These are scaled such that the median values $B_{1/2} = 1$. The delta function for $P(B_{TOT})$ and its associated $P(B_{LOS})$ are shown as thick blue lines, whereas the flat function for $P(B_{TOT})$ and its associated $P(B_{LOS})$ are shown as thin blue lines.

value B_0. $P(|B_{LOS}|)$ is now very different, with $P(|B_{LOS}|) \propto \ln(B_0/|B_{LOS}|)$. Hence, one can gain information about $P(B_{TOT})$, the distribution of the total field strengths in a sample of clouds with Zeeman observations, by comparing the observed $P(B_{LOS})$ with the $P(B_{LOS})$ predicted by various assumed $P(B_{TOT})$.

Crutcher et al. (2010) employed a Bayesian statistical technique to analyze samples of clouds with Zeeman observations in order to infer the distribution of the total magnetic field strengths in the samples. They used the four surveys (Crutcher 1999, Heiles & Troland 2004, Falgarone et al. 2008, Troland & Crutcher 2008) that had information about the volume density n_H. In addition to studies of subsets of the data, they carried out an extensive exploration over model space for all the Zeeman data, HI, OH, and CN. The model assumed was that the maximum B_{TOT} was independent of n_H up to some value of density n_0, with $B_{TOT,max} = B_0$. For $n_H > n_0$, the maximum B_{TOT} was assumed to have a power-law increase, $B_{TOT,max} = B_0(n/n_0)^{\kappa}$. A model of the PDF of B_{TOT} was used that took the form of a possible upper and lower cutoff to the flat $P(B_{TOT})$, such that the smallest $B_{TOT} = f \times B_0$ (rather than 0), with $0 \leq f \leq 1$. If $f = 1$, the PDF is a delta function, whereas if $f = 0$, then the PDF is the full flat PDF with B_{TOT} ranging uniformly between 0 and $B_0(n/n_0)^{\kappa}$. Hence, rather than two fixed $P(B_{TOT})$ (delta function and flat), the best values for four free parameters (B_0, n_0, κ, and f) were simultaneously found by the Bayesian analysis, together with the PDFs of each of these parameters. The results were $B_0 \approx 10$ μG, $n_0 \approx 300$ cm^{-3}, $\kappa \approx 0.65$, and $f \approx 0$. **Figure 6** shows the data from the four surveys and the fit from the Bayesian analysis.

The value for B_0 agrees well with a frequentist analysis of just the HI data carried out by Heiles & Troland (2005) using Monte Carlo techniques, as does the implicit conclusion that B_{TOT}(HI) does not vary strongly with n_H. The density n_o marks the value above which interstellar magnetic fields increase with increasing density. A natural explanation is that interstellar densities first increase primarily by accumulation of matter along magnetic field lines, but at the mean density $n_0 \approx 300$ cm^{-3} clouds become self-gravitating, with gravity leading to more isotropic contraction with increases in the magnetic field strength in this flux-freezing domain. Because n_0 is defined in terms of $n_H = n(\text{HI}) + 2n(H_2)$, for molecular clouds $n_0 = 300$ cm^{-3} corresponds to $n(H_2) = 150$ cm^{-3}. This is comparable with the mean density of GMCs, which are thought to be self-gravitating.

It is the other two parameters that are important for testing the role of magnetic fields in star formation. The $f \approx 0$ result confirms the result obtained from analysis of the OH and CN data alone that $P(B_{TOT})$ is flat, with magnetic field strengths in some clouds very much smaller than the mean, implying very supercritical M/Φ. New information comes from the scaling of B_{TOT} with n_H. The power-law exponent κ is significantly higher than values predicted by ambipolar diffusion theory, which has κ near zero at the beginning of the evolutionary process and approaching 0.5 in late stages (e.g., Mouschovias & Ciolek 1999). The value $\kappa \approx 0.65$ (with uncertainty $\sim \pm 0.05$) agrees with the value $\kappa = 2/3$ found by Mestel (1966) for a spherical cloud with flux freezing. The Bayesian result does not imply that clouds are spherical, merely that they are contracting such that the magnetic field is too weak to significantly impede contraction in directions perpendicular to **B**. Turbulent flows would lead to quite asymmetric clouds, as observed. Hence, the Bayesian analysis of the Zeeman data does not support the model of star formation controlled by gravity-driven ambipolar diffusion as the sole or dominant mechanism of star formation, but rather supports models in which the magnetic field is too weak to be dynamically dominant over gravity in a large fraction of molecular clouds. Of course, the Bayesian analysis does not change the fact that the mean $M/\Phi \sim 2 - 3$; some clouds have sufficiently strong magnetic fields that they are dynamically important, with ambipolar diffusion perhaps being the dominant driver of collapse in such clouds.

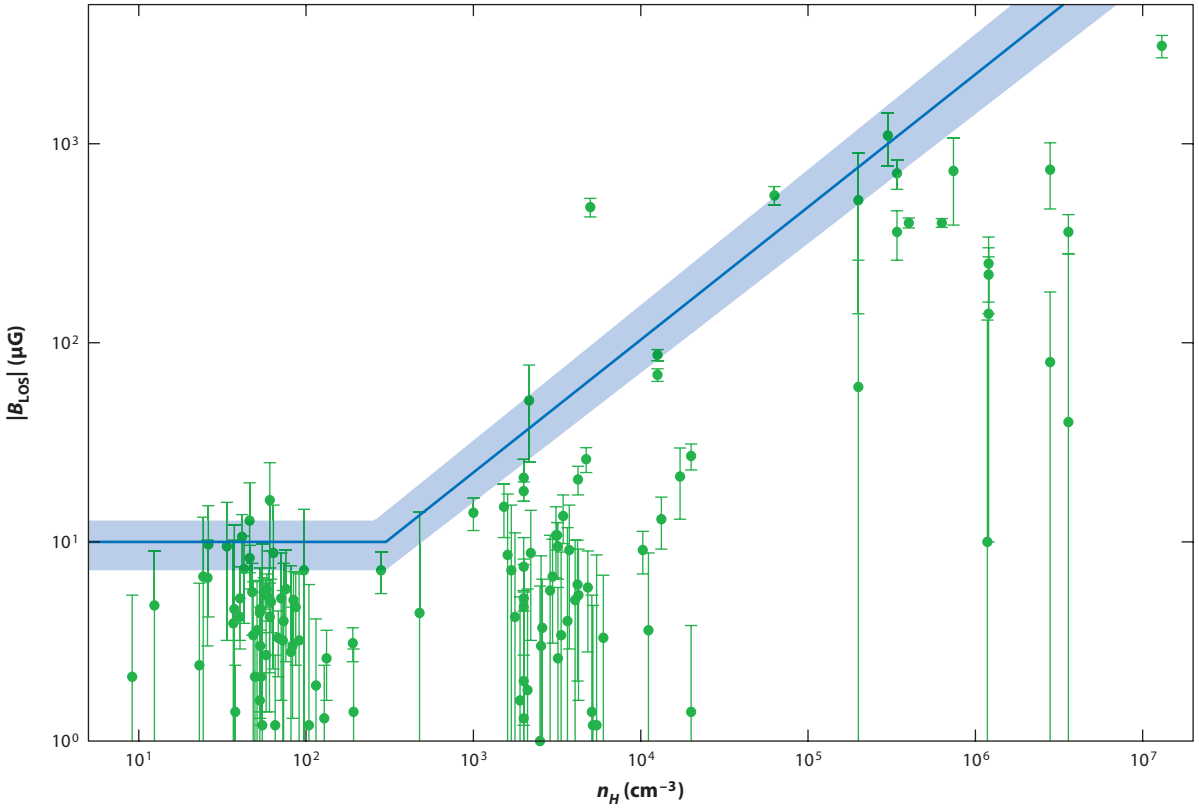

Figure 6

The set of diffuse cloud and molecular cloud Zeeman measurements of the magnitude of the line-of-sight component B_{LOS} of the magnetic vector **B** and their 1σ uncertainties, plotted against $n_H = n(\mathrm{HI})$ or $2n(H_2)$ for HI and molecular clouds, respectively (Crutcher et al. 2010). Although Zeeman measurements give the direction of the line-of-sight component as well as the magnitude, only the magnitudes are plotted. The solid blue line shows the most probable maximum values for $B_{TOT}(n_H)$ determined from the plotted values of B_{LOS} by the Bayesian analysis of Crutcher et al. (2010). Also shown (plotted as *light blue shading*) are the ranges given by acceptable alternative model parameters to indicate the uncertainty in the model.

There are additional ways to test whether ambipolar diffusion starting from magnetically subcritical clouds is the driver of star formation. **Figure 7** shows B_{LOS} versus N_H from the five major Zeeman surveys of HI, OH, and CN (Bourke et al. 2001, Heiles & Troland 2004, Falgarone et al. 2008, Troland & Crutcher 2008; K.L. Thompson, T.H. Troland, unpublished observations) and the compilation by Crutcher (1999); the straight line is for a critical M/Φ. At first glance, this figure may seem to show exactly what the ambipolar diffusion model predicts. On the left side, with $N_H \lesssim 10^{21}$ cm^{-2}, mass-to-flux ratios M/Φ are subcritical; these clouds are almost exclusively lower density HI clouds. On the right side, with $N_H \gtrsim 10^{21}$ cm^{-2}, the M/Φ are overwhelmingly supercritical; these clouds are mainly higher density molecular clouds and cores. Hence, the data appear consistent with the strong magnetic field model with neutrals gravitationally contracting, leaving the magnetic flux behind and, hence, increasing M/Φ in the higher density molecular gas. However, there are several problems with this picture. First, the cold HI clouds in the Heiles & Troland (2004) survey are in approximate pressure equilibrium with the warm ISM and are not self-gravitating, so they could not gravitationally collapse through the magnetic field. Their

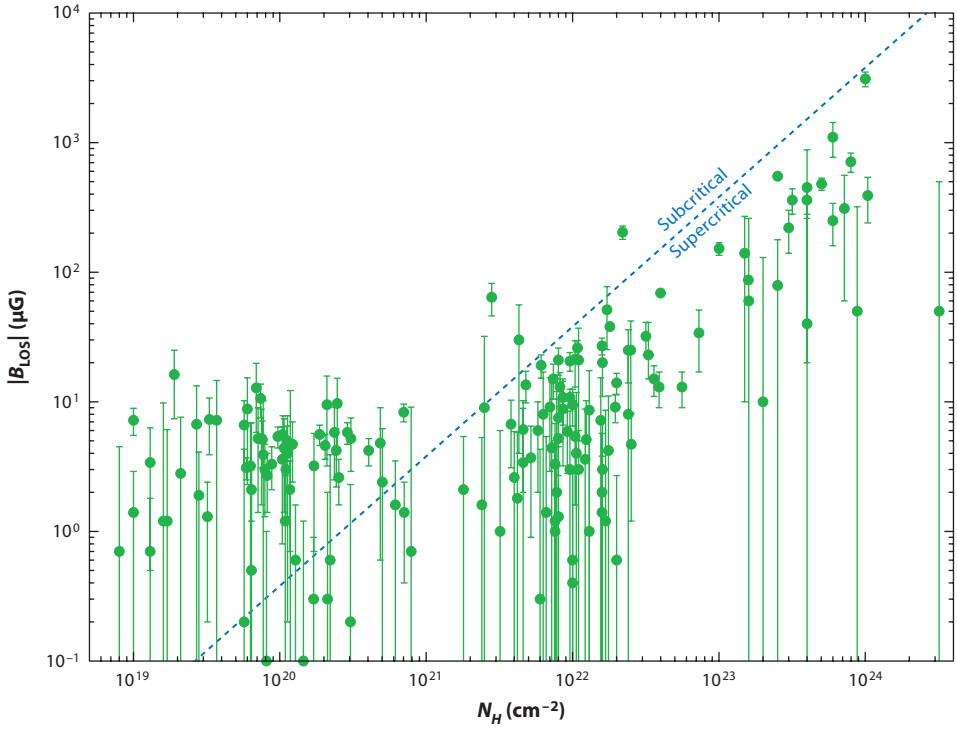

Figure 7

HI, OH, and CN Zeeman measurements of B_{LOS} versus $N_H = N_{HI} + 2N_{H_2}$. The dashed blue line is for a critical $M/\Phi = 3.8 \times 10^{-21} N_H / B$. Measurements above this line are subcritical, those below are supercritical.

analysis (Heiles & Troland 2003) showed that the structure of the HI diffuse clouds cannot be isotropic but instead must be sheet-like. Heiles & Troland (2005) found $\bar{B}_{TOT} \approx 6$ μG for the cold HI medium, a value comparable to the field strength in lower-density components of the warm neutral medium. Hence, although flux freezing applies almost rigorously during transitions back and forth between the lower density warm and the higher density cold neutral medium, the magnetic field strength does not change with density. This suggests that HI diffuse clouds are formed by compression along magnetic fields; an alternative would posit formation of clouds selectively from regions of lower magnetic field strength. They also find that the ratio of turbulent to magnetic energies is ~1.5 or approximately in equilibrium; both energies dominate thermal energy. They suggest that this results from the transient nature of converging flows, with the apparent equilibrium being a statistical result that is a snapshot of time-varying density fields.

A second argument that **Figure 7** does not show an evolutionary sequence driven by ambipolar diffusion is the lack of molecular clouds that are subcritical. Although the Zeeman measurements give directly only a lower limit to B_{TOT}, the upper envelope of the B_{LOS} defines the maximum value of B_{TOT} at each N_H; for some fraction of the clouds **B** should point approximately along the line of sight, so $B_{LOS} = B_{TOT} \cos\theta \approx B_{TOT}$ for $\theta \approx 0$. For $N_H \gtrsim 10^{21}$ cm^{-2} most of the points come from OH or CN observations; these molecular clouds are mainly self-gravitating, so this should be the region of transition from subcritical to supercritical clouds. Yet, there are zero definite cases of subcritical clouds for $N_H > 10^{21}$ cm^{-2}! The two points that seem to be above

the critical line are both from the Bourke et al. (2001) survey of OH absorption lines toward HII regions, and neither is claimed as a definite detection by these researchers. The small formal error bars do not reflect the systematic uncertainties due to OH masers within the velocity ranges of the OH absorption lines.

7.3. Masers

Finally, I briefly discuss Zeeman results for masers. Masers offer the opportunity to extend study of magnetic field strengths to higher densities and much smaller spatial scales than those sampled by the quasi-thermal, spatially extended lines of OH and CN discussed above. Important Zeeman results for the ISM have been obtained for masers of OH, H_2O, and CH_3OH, especially in high-mass star-formation regions (e.g., Vlemmings 2007). Magnetic field strengths from masers could be very useful in extending the $B \propto \rho^{\kappa}$ relation to higher densities, except that the densities of maser regions are not well known and the compression is likely most often due to shocks rather than gravity.

The interpretation of polarized maser spectra is not straightforward. A typical maser region has complex small-scale spatial and velocity structure, producing a maser spectrum with a number of blended line components with various degrees and types of polarization. In general, very long baseline (VLB) observations are necessary in order to identify spatially colocated maser spots. Then the polarization of the maser emission from each spot can be interpreted by the Zeeman effect. However, the details of maser pumping, the degree of saturation of a maser, and the propagation of polarized maser emission in a complex spatial and velocity environment produces very complicated observed Zeeman spectra. The theory of polarized maser emission and propagation is still not well understood (e.g., Watson 2009), complicating interpretation of the observations.

In principle, because OH is a paramagnetic species with large Zeeman coefficients Z, the situation for OH masers is the simplest. OH masers occur in regions of sufficiently high density ($n_H \sim 10^5 - 10^8$ cm^{-3}) that magnetic field strengths are large enough to separate the three Zeeman components (Section 6) in frequency space. However, this simple Zeeman pattern is very rarely seen due to competitive gain between the components produced by overlap of differently polarized masers and internal Faraday rotation along the line of sight (e.g., Gray & Field 1995). Spatially colocated circularly or highly elliptically polarized Zeeman pairs generally have different strengths, and the expected linearly polarized π component is rarely seen. It is therefore not possible to reconstruct the three-dimensional magnetic field from the relative intensities of the π and σ Zeeman components and the frequency separation of the σ components. The elliptically polarized colocated pairs can be interpreted as the two Zeeman σ components, and the frequency separation gives the total magnetic field strength.

The situation for H_2O and CH_3OH masers is more complicated, for the Zeeman splitting of these nonparamagnetic species is less than the line width, even for the high magnetic field strengths in these maser regions. Because of uncertain polarization propagation effects with the three Zeeman components blended together, the interpretation of the observed polarization is uncertain. Generally an observer follows the same procedure used for nonmaser lines and fits the observed Stokes V spectrum to infer B_{LOS}. But the possibly unequal strengths of the blended elliptically polarized σ components and the unknown strength of the blended π component introduce uncertainty into the inferred B_{LOS}.

Different maser transitions for OH and CH_3OH sample different densities, allowing, in principle, study of magnetic fields at different densities. OH masers at 1.6, 6, and 13 GHz sample densities $n(H_2) \sim 10^5 - 10^8$ cm^{-3}, with the densities being determined by maser theory rather than direct observation. (Because of the uncertainty in n_H, sometimes observers assume a $B \propto \rho^{\kappa}$ relationship

to estimate n_H from B_{TOT}!) Total field strengths are typically ∼1 mG, although fields of several tens of milligauss have been found. The 22-GHz H_2O maser samples $n(H_2) \sim 10^8 - 10^{11}$ cm^{-3}, again estimated from maser theory. Magnetic field strengths of $B_{LOS} \sim 15 - 150$ mG are found. Depending on the transition, CH_3OH masers at 6.7 and 12 GHz are very widely found in high-mass star-formation regions. These masers probe intermediate densities, up to $n(H_2) \sim 10^9$ cm^{-3} and give reasonable magnetic field strengths that are generally intermediate between the OH and H_2O maser results. However, Vlemmings, Torres & Dodson (2011) have pointed out that an error of one order of magnitude seems to have been made in the Zeeman coefficient Z, such that the B_{LOS} determined from the 6.7-GHz CH_3OH masers must be increased by a factor of 10, making them unreasonably large. They suggest that the CH_3OH Zeeman coefficient, currently based on not well-documented measurements 60 years ago, needs to be carefully determined before reliable magnetic field strengths can be inferred.

The W3(OH) region is an excellent exemplar of maser Zeeman studies, with the richest OH maser spectrum of any region observed to date. Reid et al. (1980) carried out the first VLB study, and Garcia-Barreto et al. (1988) the first VLB polarization study. More recently, Wright, Gray & Diamond (2004a,b, 2005) and Fish & Sjouwerman (2007) have studied the magnetic field using OH maser (1.6 GHz ground-state and 6.0 GHz excited rotational state, respectively) VLB observations and discussed the properties of the region. W3(OH) has an UltraCompact HII (UCHII) region, probably powered by a deeply embedded O7 star, surrounded by a cluster of >100 low-mass stars. There is a molecular core with $\sim 50\,M_\odot$, $n_H \sim 10^7$ cm^{-3}, $T_{kinetic} \gtrsim 100$ K embedded in a molecular envelope with $\sim 2000\,M_\odot$, $n_H \sim 10^5$ cm^{-3}, $T_{kinetic} \sim 20$ K. The OH masers are distributed over a ∼2 arcsec (∼0.02 pc) area, with distribution and velocities that generally agree with results from nonmaser studies, such as NH_3 (Guilloteau, Stier & Downes 1983), including a possible rotating dense molecular torus that may be the remnant of the flattened disk from which the O7 star formed. The OH masers appear to be behind the shock front of the expanding UCHII region. A similar core, W3(H_2O), sometimes called W3(OH)TW, is 6 arcsec (0.06 pc) east of W3(OH). It has H_2O masers but weak OH masers and no UCHII region; hence, it appears to be at a slightly earlier evolutionary stage.

Several hundred OH maser Zeeman pairs have been identified in W3(OH), allowing a detailed study of the magnetic field in the dense gas. Wright, Gray & Diamond (2004b) produced a contour map of $|\mathbf{B}|$ over a $\sim 0.015 \times 0.022$ pc area. The magnetic field points away from the Sun over most of the area, except in the extreme east and southeast. A toroidal magnetic field could explain the field reversal. The field strength maximum is ∼12 mG, near the northern limit of the UCHII region and the putative molecular torus; the typical strength is ∼4–6 mG, with considerable small-scale structure. If we take 5 mG for the typical magnetic field strength and an H_2 column density $N \approx 10^7$ cm^{-3} × 0.02 pc $\approx 6 \times 10^{23}$ cm^{-2}, we find that M/Φ is approximately critical; the field is sufficiently strong to support the molecular core against gravity. However, even though the maser OH Zeeman result gives directly the total magnetic field strength, the appropriate value for the column density is highly uncertain, and thus so is M/Φ.

There are a large number of CH_3OH masers of both collisional excitation in shocks and radiative excitation types. The CH_3OH masers sample a wide range of physical conditions. Vlemmings, Harvey-Smith & Cohen (2006) observed CH_3OH 6.7-GHz masers, which occur in regions with similar densities and temperatures to the 18-cm ground-state OH masers. They detected linear polarization with similar position angles over most of the region; when Faraday rotation is taken into account, the data agree with position angles measured in ground-state OH masers and indicate a position angle for the plane-of-sky magnetic field of ∼10°–15°, which is parallel to the long north-south filament that has been interpreted as a rotating dense molecular torus. This field morphology would be consistent with the model of compression behind a shock generated by the

UCHII region. However, because of uncertain maser propagation effects, it is not certain whether the π or σ Zeeman components (Section 6) dominate the linear polarization, so there is a 90° ambiguity in magnetic field direction that complicates the interpretation.

The W3(H_2O) core has strong H_2O masers and only weak OH masers. Alcolea et al. (1993) have measured the proper motions of the individual maser components and have shown that they are part of a bipolar outflow expanding at about 20 km s^{-1}. Wilner, Reid & Menten (1999) found continuum emission peaks at 8.4 GHz within the H_2O maser region that they interpreted as a synchrotron jet. They suggested that secondary peaks at the extrema of the H_2O maser distribution mark the locations of deeply embedded Herbig-Haro objects that resulted from strong shocks. A.P. Sarma, K. Weiler, M. Pastorius, E. Momjian, J.D. Romney, and T.H. Troland (unpublished observations) have measured the Zeeman effect with the Very Long Baseline Array in 14 Zeeman pairs, 13 of them located in the eastern area of the H_2O maser distribution, and found $B_{LOS} = 13 - 85$ mG, with $\bar{B}_{LOS} = 33$ mG. There is no preferred sign of the inferred B_{LOS}, which suggests that the outflow is close to the plane of the sky so that B_{LOS} is oppositely directed on the front and back of the outflow. If so, B_{TOT} would be quite large.

W3(OH) shows both of the configurations that have been suggested for the location of masers in high-mass star-formation regions. One is behind shocks generated by the expansion of UCHII regions; the other is associated with outflows. In both cases, mechanical compression of the gas led to conditions favorable for the maser emission, with the high magnetic field strengths being at least partially due to high gas densities that were not produced directly by gravitational contraction of molecular clouds.

Masers also offer the opportunity to study the Galactic-scale morphology of magnetic fields. When linear polarization is detected, it is possible to map B_{POS}. But studies of the direction of B_{LOS} (toward or away from the Sun) are also useful in studying the larger-scale Galactic magnetic field. Reid & Silverstein (1990) suggested from OH maser studies that the magnetic field direction in the Solar Neighborhood is largely preserved during contraction from interstellar densities to those of OH masers near newly formed massive stars; extension to additional maser observations supported this idea (e.g., Fish et al. 2003; Caswell, Kramer & Reynolds 2011), although there are regions where the field is reversed with respect to the ordered direction. These data suggest that the strength of the magnetic field is sufficient to play a significant role in the formation of molecular clouds (such as flows within flux tubes) and that the field direction is not significantly affected during the formation of high-density cores within them.

8. GOLDREICH-KYLAFIS (GK) EFFECT: TECHNIQUE

Linear polarization may also arise in nonmaser lines (Goldreich & Kylafis 1981, Kylafis 1983), an effect that has become known as the Goldreich-Kylafis (GK) effect. Deguchi & Watson (1984) extended the analysis by including more than two excitation levels in order to improve the theoretical predictions. If (even very small) Zeeman splitting has removed the degeneracy of magnetic sublevels in a molecule, the molecule can emit or absorb only linearly polarized radiation perpendicular to **B** (σ transitions) or parallel to **B** (π transition) and circularly polarized radiation parallel to **B** (σ transitions). If the excited states of the molecule are populated by anisotropic radiation, magnetic sublevels will have populations differing from thermal equilibrium values. The anisotropic radiation can be either external or internally generated by trapping of line photons within a region that has a velocity gradient so that the line optical depth is anisotropic. Then radiative de-excitation will produce a net linearly polarized spectral line.

A simple example can illustrate this. Collisional excitation of CO will populate the magnetic substates in equilibrium, and there will be no net polarization. But suppose collisional excitation

is dominated by trapping of line photons. If the velocity gradient is larger perpendicular to **B** (as predicted for MHD turbulence), the line optical depth will be smaller perpendicular to **B**. Because radiative excitation of the $M = 0$ state is only by π transitions perpendicular to **B**, whereas excitation of the $M = \pm 1$ states is by σ transitions both parallel and perpendicular to **B**, the population of the $M = \pm 1$ states will be enhanced due to the larger line optical depth parallel to **B**. Hence, the observed σ radiation from the $M = \pm 1$ states will be stronger than the π radiation, and the combined radiation will be linearly polarized perpendicular to **B**.

More generally, molecular lines will have net linear polarization either parallel to B_{POS} ($M = 0$ overpopulated) or perpendicular to B_{POS} ($M = \pm 1$ overpopulated) depending on the generally unknown angles between the magnetic field, the direction of the radiation anisotropy, and the line of sight. Hence, observation of linearly polarized lines has a 90° ambiguity in determining B_{POS}. Because the circularly polarized $\pm\sigma$ components along the line of sight are equal in strength, no net circular polarization is observed. Only the relatively large frequency splitting of the $\pm\sigma$ components by paramagnetic molecules allows detection of the change in circular polarization across the line profile—the Zeeman effect.

The GK effect may be used to probe magnetic field morphologies in molecular clouds; linearly polarized lines may be observed toward molecular clouds, where dust emission is too faint for polarimetry because detection of dust emission requires larger total column densities than detection of molecular line emission. The linearly polarized line emission requires that radiative excitation dominate collisional excitation and that the line optical depth be ∼1. Hence, different molecular transitions may be used to probe **B** in different regions within molecular clouds. Hence, in spite of the 90° ambiguity in the direction of B_{POS} from the GK effect, this technique provides a valuable additional tool for studying magnetic fields in regions of star formation. The CF technique may be applied to GK maps of polarization vectors to estimate field strengths.

9. GK EFFECT: OBSERVATIONAL RESULTS

The first attempt to detect the GK effect in molecular clouds was unsuccessful (Wannier, Scoville & Barvainis 1983), in spite of the fact that sensitivity to linearly polarized molecular lines significantly below predicted values was achieved. Although Deguchi & Watson (1984) showed that including all relevant levels of excitation would significantly decrease the predicted level of linear polarization, searches for the GK effect did continue until success was achieved by Glenn et al. (1997) in extended envelopes of evolved stars and by Greaves et al. (1999) in molecular clouds. They attributed their success to observing regions with line optical depth ∼1 rather than cloud cores, controlling instrumental polarization problems, and having more sensitive receivers. Detections at the fractional linear polarization level of ∼1% were made toward the Galactic center, S140, and DR21 molecular clouds in the lines CO $J = 2-1$ and $J = 3-2$ and ^{13}CO $J = 2-1$. The linear polarization directions obtained from the spectral lines agreed with those from dust emission.

Greaves, Holland & Ward-Thompson (2001) used the GK effect to measure the magnetic field direction in the NGC 2024 molecular outflow, finding that the outflow direction was parallel to B_{POS} and arguing that the magnetic field could be channeling the magnetized outflow. They resolved the 90° ambiguity in the position angle of B_{POS} by noting that the one-dimensional velocity field of the outflow would provide the anisotropy in line optical depth that is necessary for the GK effect to occur. They estimated theoretically that a field strength $B \gtrsim 35 - 70$ μG should be sufficient to keep the flow well collimated. Greaves, Holland & Dent (2002) used the ability to probe the velocity structure of magnetic fields by studying the field directions just north of Sgr A*. By separating the rotating circumnuclear disk and the in-falling streamers by velocity, they showed that the -20 km s^{-1} streamer has a different magnetic field from that of the circumnuclear

disk and that there is no clear correlation with the gas flow directions. They noted that a more extensive CO polarization map together with 3D reconstructions of the various molecular clouds would make it possible to produce a 3D magnetic field map within a few parsecs of Sgr A*; this has not yet been done.

Interferometric observations of the GK effect make it possible to map magnetic field morphologies with higher angular resolution than that achieved in the above single-dish (JCMT) observations. The first such observations came almost simultaneously with the JCMT single-dish detection; Girart, Crutcher & Rao (1999) used the BIMA interferometer array to map polarized dust emission in the molecular core NGC 1333 IRAS4A and CO $J = 2 - 1$ polarized line emission in the molecular outflow. They found that close to the core the outflow is at an angle $\sim$50° to both the magnetic field and the minor axis of the molecular core. About 0.03 pc from the center of the core the outflow direction bends in the direction of the magnetic field, a result predicted by theory for a flow direction that differs from the magnetic field direction (Hurka, Schmid-Burgk & Hardee 1999) for a flow velocity $\sim$10 km s^{-1} and a magnetic field strength $\gtrsim$ 150 μG.

Girart et al. (2004) combined JCMT single-dish data with BIMA interferometer array data to produce a fully spatially sampled map of the OMC1 molecular cloud as a function of radial velocity. **Figure 8** shows the results. **Figure 8*a*** shows that the fractional polarization increases from line center to line wings, as expected because linear polarization is a maximum for line optical depth $\tau \sim 1$, and that the position angle of the polarization varies with velocity across the line, indicating that B_{POS} is a function of velocity. To the extent that a velocity model of a region can be constructed, these data, together with Zeeman data, could be used to construct a 3D model of **B**. The CO polarization maps can be compared with similar maps of dust continuum polarization made with similar spatial resolution (Rao et al. 1998). At the northeastern position (with respect to the IRc2), the CO and dust polarization vectors are parallel within the errors. However, for the positions closer to the center of the map the CO polarization vectors are neither perpendicular nor parallel to those of the dust polarization. Indeed, the difference between the CO and dust position angles is roughly 40°. This suggests that the redshifted and blueshifted CO and the dust emission trace different spatial regions along the line of sight. The redshifted and blueshifted CO maps probably trace the molecular outflow. Thus, the well-ordered and uniform magnetic field inferred from the CO polarization maps imply that the molecular outflow is embedded in a region with a strong magnetic field.

Other BIMA maps of CO polarization were severely limited by noise, but provided additional information about the relationship between magnetic fields and molecular outflows. Cortes, Crutcher & Matthews (2006) mapped a second bipolar outflow (NGC 2071IR) in the linearly polarized emission from the CO $J = 2 - 1$ line. They found the line polarization in the red lobe of the outflow to be orthogonal to that in the blue lobe, a result that is consistent with the GK mechanism. Kwon et al. (2006) detected linearly polarized CO $J = 2 - 1$ emission toward the multiple protostar system L1448 IRS3, a region with two outflows. For both sources, the CO polarization was consistent with a magnetic field parallel to an outflow. Cortes et al. (2008) mapped dust and CO $J = 1 - 0$ linearly polarized emission toward the massive star-forming region G34.4+0.23 MM. This region has a filamentary morphology with the magnetic field orthogonal to the long axis of the filament. Because the CO $J = 1 - 0$ polarization samples the magnetic field in lower density [$n(H_2) \sim 100$ cm^{-3}] envelope regions that are apparently dominated by outflows while dust emission polarization samples high density regions, these results imply a fairly uniform field morphology. However, the magnetic field in individual outflows was not spatially resolved. The summary of the CO polarization results to date is that molecular outflows are along the magnetic field direction, consistent with the outflows being powered by magnetocentrifugal forces and guided by the magnetic field at larger scales.

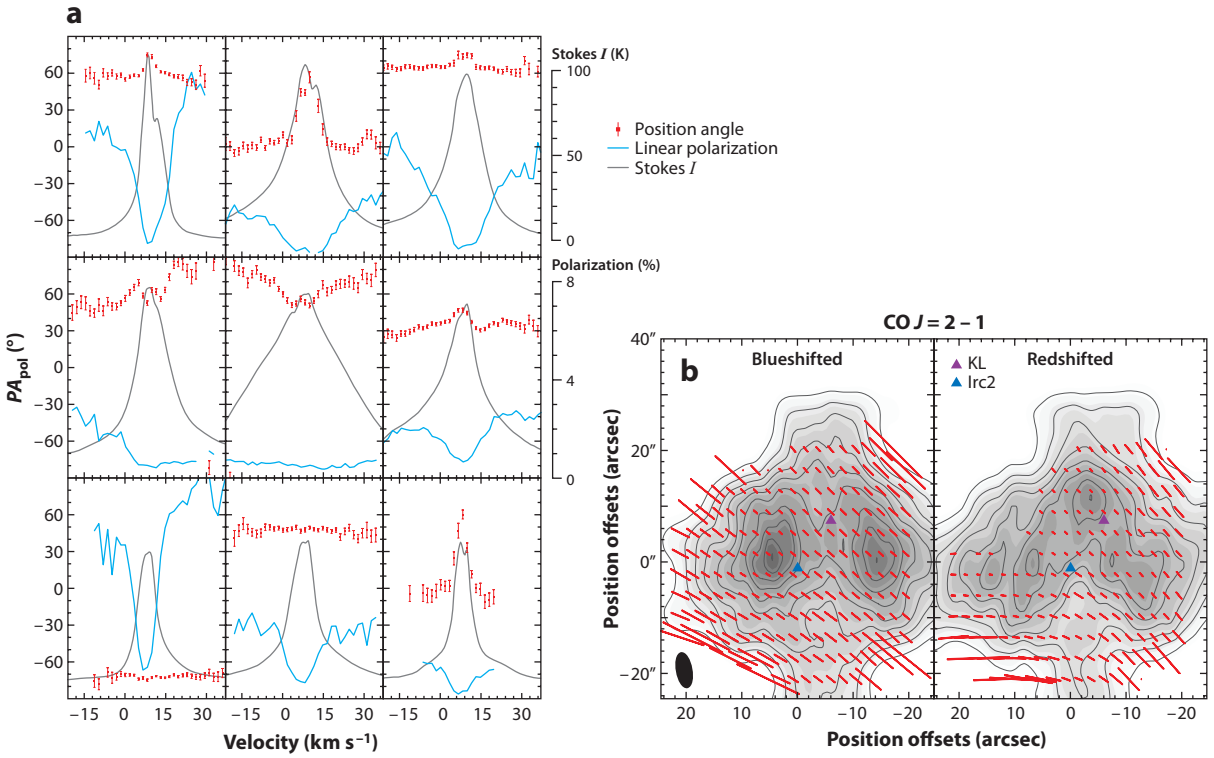

Figure 8

Goldreich-Kylafis effect line profiles and maps of magnetic fields toward OMC1 (Girart et al. 2004). Panel *a* shows Stokes *I* profiles at nine positions with the fractional linear polarization and the polarization position angle as functions of velocity superposed. Panel *b* shows maps of the linear polarization position angle and fractional polarization; the left map is of blueshifted ($v_{LSR} = -5$ km s^{-1}) gas and the right map is of redshifted ($v_{LSR} = +23$ km s^{-1}) gas, each covering 16 km s^{-1}. The gray scale is the CO $J = 2 - 1$ emission, whereas triangles show the positions of the KL (*purple upper right*) and IRc2 (*dark blue lower left*) objects.

Lai, Girart & Crutcher (2003) used BIMA to map CO $J = 2 - 1$ polarized emission toward DR21(OH), finding that the magnetic field sampled by CO is parallel to the field they mapped with polarized dust emission at $\lambda \approx 1$ mm; however, the CO polarization covered a wider area, consistent with the CO sampling a lower density envelope surrounding the binary core imaged by dust emission. This conclusion is also consistent with the requirements for GK line polarization. Subsequent mapping of the CO $J = 1 - 0$ polarized emission found the unexpected result that the CO $J = 2 - 1$ and $J = 1 - 0$ polarization directions were orthogonal (Cortes, Crutcher & Watson 2005). They carried out numerical multilevel full polarization radiative transfer calculations to model DR21(OH). Their model had a smaller velocity gradient along **B** characteristic of MHD turbulence (Goldreich & Sridhar 1995); **B** itself was orthogonal to the direction toward the dense core. They found that the observations could be explained if two different molecular radiative excitation mechanisms were in play. One is anisotropic line optical depths due to a velocity gradient in the gas (the usual GK effect mechanism), whereas the other is radiative excitation of the CO levels by continuum emission from dust grains in the core. Because the latter emission would be anisotropic as seen from the lower density region surrounding the core, it could also produce the required anomalous populations of the magnetic sublevels.

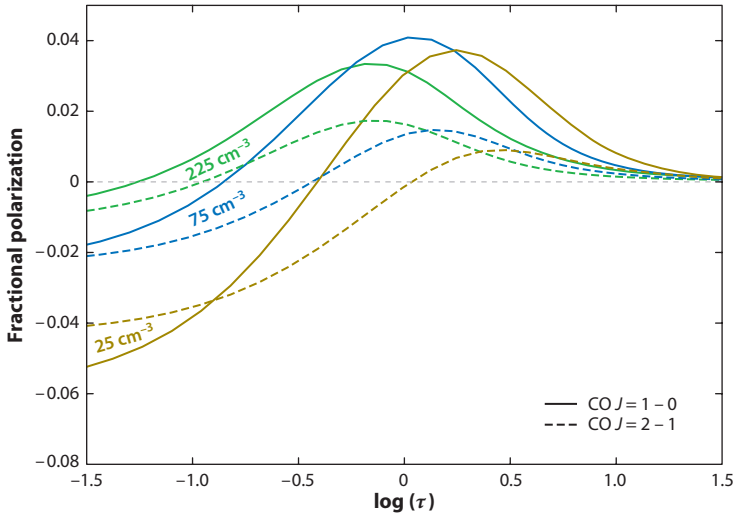

Figure 9

Calculations of the polarization of CO $J = 2$–1 and 1–0 lines toward DR21(OH) produced by radiative excitation (including the effect of cosmic microwave background radiation). The abscissa is the optical depth of the $J = 1$–0 transition. Positive (negative) fractional polarization is perpendicular (parallel) to the local magnetic field. Results for three values of the local $n(H_2)$ are shown (Cortes, Crutcher & Watson 2005).

Figure 9 shows the result of the modeling. This figure is instructive in understanding how the GK effect works. At very small CO line optical depths, the effect of the anisotropic line optical depths is not important and the radiative excitation by the central source of millimeter-wave photons dominates. Because this excitation source is perpendicular to the magnetic field in the region of CO emission, the excitation of the $M = \pm 1$ magnetic sublevels that would occur by absorption of circularly polarized radiation parallel to **B** will not occur, the $M = 0$ state will be preferentially populated, and the resultant CO emission is linearly polarized parallel to the magnetic field direction ($p < 0$ in **Figure 9**). As the model line optical depth is increased, the effect of the velocity gradient (that is smaller parallel to **B**) becomes important, and radiative de-excitation will be reduced more parallel to **B** than perpendicular to **B**. Because radiative de-excitation of the $M = \pm 1$ sublevels is decreased more by radiation trapping compared with the $M = 0$ substate, the radiation will be linearly polarized perpendicular to **B** ($p > 0$). However, because the dust radiation from the core is much weaker at the 115-GHz frequency of the $J = 1$–0 transition than at the 230 GHz frequency of the $J = 2$–1 transition, the external radiation will play a lesser role for the polarization of the $J = 1$–0 transition than for the $J = 2$–1 transition. Hence, as seen in **Figure 9**, the $J = 1$–0 transition polarization begins to switch from negative (parallel to **B**) to positive (perpendicular to **B**) at lower line optical depths. The effect of the anisotropic line optical depth due to the velocity gradient is at a maximum around $\tau(CO) \sim 1$. At large line optical depths, the effect of the velocity gradient goes away because $\tau(CO) \gg 1$ in all directions, and photon trapping will equilibrate the magnetic sublevels. Collisions will also tend to equilibrate the magnetic sublevels, so the density must be moderate, $n(H_2) \sim 100$ cm^{-3}. As shown in **Figure 9**, the higher the density at any line optical depth, the smaller the GK effect. Similar observations toward other molecular clouds can be an important informant of physical conditions.

10. A DIRECT TEST OF AMBIPOLAR DIFFUSION

Crutcher, Hakobian & Troland (2009) carried out a direct observational test of a prediction of the ambipolar diffusion theory. The prediction tested was that ambipolar diffusion will produce an increase in M/Φ from the envelope-to-core region of a cloud. This is a fundamental aspect of the theory, so observing (or not) this prediction provides a direct test of the theory. As noted above, Zeeman observations give only the line-of-sight component of **B**, so any individual measurement of M/Φ gives only an upper limit. Hence, for any individual case, one would need to be able to determine the angle θ between the magnetic field vector and the line of sight to find the true value of M/Φ. However, for a test of the ambipolar diffusion prediction, it is only necessary to determine the change in M/Φ from an envelope region to a core region of a cloud whose contraction was being driven by ambipolar diffusion, or $\mathcal{R} \equiv [M/\Phi]_{core}/[M/\Phi]_{envelope}$. The idealized ambipolar diffusion theory of core formation requires $\mathcal{R}$ to be approximately equal to the inverse of the original subcritical M/Φ, or $\mathcal{R} > 1$.

To test this prediction, Crutcher, Hakobian & Troland (2009) selected four dark clouds from the Troland & Crutcher (2008) OH Zeeman survey that had strong detected B_{LOS} and carried out OH Zeeman observations toward the envelope regions surrounding the dark cloud cores in order to measure $\mathcal{R}$. The central assumption was that the angle θ between the line of sight and the magnetic field was approximately the same between core and envelope. Then the measured $B_{LOS} = B_{TOT}\cos\theta$ would have the same θ in the numerator and denominator of $\mathcal{R}$, and the dependence on the unknown θ would disappear. Because clouds with the strongest measured B_{LOS} were selected, it is likely that $B_{LOS} \approx B_{TOT}$ with $\theta \sim 0$, so $\cos\theta \approx 1$ and small changes in θ between core and the envelope positions would not affect $\mathcal{R}$ very much. Supporting this assumption of the experiment is the fact that published models of core formation driven by ambipolar diffusion have strong, regular magnetic field morphology such that the unknown angle θ between **B** and the line of sight is approximately the same in core and envelope regions. Using the same Zeeman tracer (OH) for the core and envelope measurements also significantly reduced dependence on $[X/H_2]$ (where X is the Zeeman species) in inferring M/Φ, because only the ratio of the M/Φ was measured.

Surprisingly, the experiment was unable to detect the Zeeman effect toward 15 of the 16 envelope positions, in spite of having excellent sensitivity. Nonetheless, the observations gave values for B_{LOS} and their uncertainties averaged over each envelope. Together with the earlier measurements of B_{LOS} toward each core position and the ratio of $N(OH)$ toward each core and envelope, it was possible to infer $\mathcal{R}$ and its uncertainty toward each cloud. Because of the failure to achieve significant detections of B_{LOS} in the envelopes, in no case was the value of $\mathcal{R}$ significantly different from 0; but the astrophysical question is whether the $\mathcal{R}$ were significantly different from 1 because the ambipolar diffusion theory requires that $\mathcal{R} > 1$. The results for the four clouds (two prestellar and two protostellar) were: $\mathcal{R}(L1448CO) = 0.02 \pm 0.36$, $\mathcal{R}(B217-2) = 0.15 \pm 0.43$, $\mathcal{R}(L1544) = 0.42 \pm 0.46$, and $\mathcal{R}(B1) = 0.41 \pm 0.20$. Hence, in all four cases, the measured $\mathcal{R} < 1$, not >1 as ambipolar diffusion predicts. In two cases, $\mathcal{R} < 1$ at near a 3σ level.

Lunttila et al. (2009) "observed" in a computer one of their super-Alfvénic (weak magnetic field) simulations of cloud formation and obtained OH Stokes I and V spectra for their cores and envelopes with exactly the instrumental parameters of the Crutcher, Hakobian & Troland (2009) experiment. They found that the observational results were very well reproduced in this weak-field model, which gives a wide range in $\mathcal{R}$ from core to core but strongly favors $\mathcal{R} < 1$.

Magnetic reconnection (Lazarian 2005) could also explain the Crutcher, Hakobian & Troland (2009) results. Because magnetic reconnection will be fastest in more turbulent and larger-scale regions, it would lead preferentially to loss of magnetic flux in the envelopes of molecular clouds

compared with core regions. Hence, $\mathcal{R} < 1$ would be due to decrease in magnetic field strengths in envelopes, as observed by Crutcher, Hakobian & Troland (2009).

Proponents of the ambipolar diffusion theory strongly attacked the Crutcher, Hakobian & Troland (2009) results and conclusion, with the two strongest objections being that (*a*) motion of cores through surrounding more-diffuse gas could lead to **B** in cores and their envelopes not being essentially parallel and (*b*) that, because B_{LOS} was not detected in the envelopes, only upper limits should be considered (Mouschovias & Tassis 2009, 2010). Crutcher, Hakobian & Troland (2010) responded to the objections. The first objection is certainly possible, but evidence discussed above that B_{POS} directions in cores and surrounding gas are strongly correlated (e.g., Li et al. 2009) argues against this. On the second objection, it is certainly true that, at the 3σ upper-limit level, $\mathcal{R} > 1$ is consistent with the data for each cloud individually, but the probability that all four of the clouds have $\mathcal{R} > 1$ is 3×10^{-7}. In any case, one fact is clear—the experiment did not provide observational support for the ambipolar diffusion theory, and it was designed to produce such support if it existed for these four low-mass cores.

11. MODELS OF SPECIFIC CLOUDS

Ambipolar diffusion models have been calculated specifically for two clouds for comparison with observational data including OH Zeeman detections. Crutcher et al. (1994) discussed a model specifically for B1; it had a core mass of 13 $M_\odot$, an envelope mass of 600 $M_\odot$, an envelope radius of 2.9 pc, an initial central $B_{TOT} = 43$ μG, and an initial central $M/\Phi = 0.42$ of critical. The model assumed that the cloud was a disk whose minor axis was at an angle $\theta = 70°$ to the line of sight; all observed properties of B1 available at that time were given accurately by the model. In particular, the present-day ambipolar diffusion evolved central $B_{LOS} = 29$ μG; the observed value is $B_{LOS} = 27$ μG. The prediction of this model would be $\mathcal{R} = 1/0.42 = 2.4$, a factor of ∼6 larger than the result above for B1. Moreover, now that the Troland & Crutcher (2008) survey of dark cloud cores has shown that B1 has the greatest B_{LOS} of any core with a detected B_{LOS}, it seems more likely that **B** is nearly along the line of sight and that the true central B_{TOT} is close to the observed $B_{LOS} = 27$ μG and not the model result $B = 85$ μG, which implied $B_{LOS} = 85$ μG $\cos 70° = 29$ μG. When B1 was among a very small number of dark clouds with sensitive OH Zeeman observations, it was not unreasonable to hypothesize that its field lay nearly in the plane of the sky. However, other clouds similar to B1 with similar total field strengths should have **B** nearly along the line of sight, yielding $B_{LOS} \sim 85$ μG; these are not found in Troland & Crutcher's (2008) survey results.

Ciolek & Basu (2000) computed a model for L1544. The model had 30 $M_\odot$ within a radius of 0.45 pc, with additional mass that does not participate in the evolution in the envelope at larger radius (not clearly specified, but apparently about 2.5 pc based on their figure 1c). They assumed $\theta \approx 74°$, again a very large angle between **B** and the line of sight, which was necessary in order to have the required large central field strength agree with the small observed value of B_{LOS}. The initial M/Φ was 0.8 of critical. This would imply $\mathcal{R} \approx 1.25$, which differs from the measurement (see previous section) of $\mathcal{R} = 0.42 \pm 0.46$, although not by a highly significant amount. However, as for B1, the large value for θ they had to assume in order to make the field strength of the model agree with the observation of B_{LOS} seems unreasonably large.

12. FARADAY ROTATION

The position angle of linearly polarized radiation will be rotated by passage through an ionized medium by an angle proportional to $n_e B_{LOS} L \lambda^2$, where n_e is the electron density, L is the path

length, and λ is the wavelength of the radiation. Because molecular clouds have a low fractional ionization and would generally have a small path length, Faraday rotation would not normally be expected in molecular clouds. However, Wolleben & Reich (2004) found highly structured, frequency-dependent linearly polarized continuum emission features in their λ 18-cm and λ 21-cm maps toward the Taurus molecular clouds, with polarization minima with excessive rotation measures at the cloud boundaries. They modeled these rotation measures as an effect of Faraday screens at the surfaces of the molecular clouds. Using upper limits to the electron density from *Hα* observations, they concluded that $B_{LOS} > 20$ μG.

Because this technique would be an important addition to the small set of tools available for studying magnetic fields in molecular clouds, Crutcher & Troland (2008) attempted to verify the magnetic field interpretation by searching for the Zeeman effect in OH lines from the molecular cloud. Only the position from Wolleben & Reich (2004) with the strongest OH lines was observed for the Zeeman effect. The OH Zeeman result was $B_{LOS} = +5 \pm 5$ μG, a nondetection that is at least 3σ below the $B_{LOS} > 20$ μG result inferred from the Faraday screen model. Robishaw (2008) also attempted to verify the Wolleben & Reich (2004) result with HI Zeeman observations toward three positions and set an upper limit of ∼5 μG for Taurus dark cloud gas at $v_{LSR} \approx$ 8–10 km s^{-1}. However, they did detect $B_{LOS} \approx 35 - 40$ μG toward the Taurus positions in an HI component at −50 km s^{-1} and suggested that the Faraday screens may be associated with this HI gas that is unassociated with the Taurus molecular gas.

13. WIDTHS OF NEUTRAL AND IONIZED MOLECULAR LINES

Houde et al. (2000a) introduced a method that did not involve polarimetry for studying magnetic fields in molecular clouds. They suggested that, in the presence of turbulence and magnetic fields, ions would be inhibited from moving across magnetic field lines but would follow gyromagnetic motion around the field, whereas neutrals would be free to move independently of the direction of the magnetic field. For a sufficiently strong **B** an ion's mean velocity perpendicular to the field would be negligibly small. Hence, ions would have a smaller line width than would neutrals. Observations of a neutral and an ionized species (such as HCN and HCO^+) that could be argued to be located in the same region of a molecular cloud could then lead to the conclusion that a strong magnetic field was present. Houde et al. (2002) argued that since a dominant regular magnetic field would lead to the same line widths for observations along the field and much narrower HCO^+ than HCN lines for observations orthogonal to the field, the angle between the line-of-sight and plane-of-sky components of **B** could be inferred. Li & Houde (2008) extended this approach by considering the turbulent velocity dispersion spectra of ion and neutral species, arguing that the line width difference was due to a turbulent ambipolar-diffusion range within which ion and neutral turbulent energies dissipate differently. They also argued that B_{POS} and the angle between the field and line of sight could not be inferred independently from line width data alone. With the assumption that turbulent ambipolar diffusion is responsible for the narrower line widths of ions, they showed that one can infer the ambipolar decoupling scale and obtained the first result of 1.8 mpc (370 AU) in M17, in agreement with theoretical expectations (Lazarian, Vishniac & Cho 2004; McKee & Ostriker 2007); they also estimated the plane-of-sky magnetic field strength B_{POS}.

Houde et al. (2000a) applied the technique of comparing widths of ionized and neutral molecular lines to observations of HCN, HCO^+, and N_2H^+ lines toward four molecular clouds, finding that the ion lines were significantly narrower than the neutral line and arguing that this was due to the presence of a magnetic field. Houde et al. (2000b) found the same result for lines of $H^{13}CN$ and $H^{13}CO^+$ toward 10 clouds and argued that optical depth effects were not responsible for the

narrowing of ion lines. Houde et al. (2002) applied this technique to M17, combining Zeeman, dust polarization, and line width maps to derive a map of the angle θ between **B** and the line of sight. This angle varied over the map, but was typically $\theta \lesssim 60°$. Because the Zeeman measurements gave a maximum $B_{LOS} \approx -750$ μG, the total field strength would be about 1.5 mG. Toward positions in the Orion A molecular cloud, Houde et al. (2004) found that $60° < \theta < 80°$ for different regions. Kirby (2010) used the line width technique for the DR21 Main molecular cloud to estimate θ. Using this together with other data, he presented a 3D hourglass magnetic field model of the cloud, with equilibrium between gravity and magnetic and kinetic energy support.

This technique was tested numerically by Falceta-Gonçalves, Lazarian & Houde (2010). The effect has also been observed through brute-force two-fluid simulations (i.e., no heavy ions approximation) using realistic ionization fractions (Tilley & Balsara 2010). These tests agreed with observations. At this time the line width technique seems promising, but questions about its theoretical foundation and the requirement for the colocation of the neutral and ionized species remain that limit its acceptance.

SUMMARY POINTS

1. The two most crucial issues are the relative importance of turbulent energy to magnetic energy (whether clouds are super- or sub-Alfvénic) and of gravitational energy to magnetic energy (whether clouds are magnetically supercritical or subcritical). The observations paint a complex picture.
2. The relative importance of turbulent to magnetic energy is addressed by a number of linear polarization results. The observed column density power spectrum in several cloud complexes is best reproduced by simulations that are super-Alfvénic, but agreement in the mean alignment of fields in cores and the surrounding medium cannot be reproduced by globally super-Alfvénic cloud models. Magnetic field morphologies appear to be generally fairly smooth and coherent from the Galactic to the molecular core scales. The general coherence of the field direction over many scale sizes certainly suggests that magnetic energy is non-negligible in molecular clouds. Ordered fields can be either along filamentary structures, suggesting matter contained by magnetic flux tubes, or perpendicular to elongated structures, suggesting contraction along magnetic field lines. Intermediate orientations can be partially due to projection effects, but must in some cases be real. However, a minority of regions do have an apparent chaotic field structure.
3. A Bayesian analysis of molecular Zeeman results suggests that, at any given density, the field strength can have a wide range of values; clouds where the field is weak would be super-Alfvénic. However, most molecular clouds have sufficiently strong magnetic fields that turbulent and magnetic energies are comparable; in some cases, magnetic energy dominates turbulent energy.
4. The maximum strength of the interstellar magnetic field seems to be fairly constant at ∼10 μG up to densities $n_H \sim 300$ cm^{-3}. The observational data seem generally consistent with the scenario that molecular cloud complexes are formed by accumulation of matter along magnetic flux tubes, so the magnetic field does not increase significantly with density.

5. At densities $n_H \gtrsim 300$ cm^{-3}, the magnetic field strength increases with increasing density with a power-law exponent $\kappa \approx 2/3$, which is expected if gravity dominates the magnetic pressure. The mean mass-to-flux ratio $M/\Phi \approx 2 - 3$ (supercritical), which implies that magnetic pressure is insufficient to balance gravity and prevent contraction. Hourglass magnetic field morphologies are found in a few cases, which is a clear signature of gravitational contraction with the larger-scale regular field dominating the turbulent field. However, the mean M/Φ in molecular clouds is only slightly supercritical, and magnetic field strengths appear to vary considerably from cloud to cloud, so some clouds may be magnetically supported. There is no definitive evidence for subcritical molecular clouds or for ambipolar-diffusion-driven star formation. Magnetic reconnection rather than ambipolar diffusion may be principally responsible for reducing M/Φ.
6. Observations of maser polarization have shown that magnetic field strengths continue to increase with density, up to ~100 mG. However, uncertainties in the theory of maser polarization limit the usefulness of maser polarization for study of magnetic fields in molecular clouds.

FUTURE ISSUES

1. New polarization capabilities and new telescopes with greater sensitivity will soon be available that will greatly extend our knowledge of magnetic fields in molecular clouds. These include the SCUBA2 polarimeter on the JCMT and polarimetry capability on CARMA and Plateau de Bure, a polarimeter on the HAWC camera on SOFIA, all-sky submillimeter polarimetry with the Planck satellite, and the Atacama Large Millimeter Array for high-resolution polarimetric imaging of dust continuum emission and spectral-line Zeeman and GK effects.
2. Although considerable observational data on magnetic fields in molecular clouds have been obtained, astrophysical conclusions remain tentative. Additional observational work that can solidify our understanding of the role of magnetic fields in star formation includes: (*a*) measurement of the overall M/Φ of molecular cloud complexes to see if they are magnetically supported; (*b*) additional Zeeman measurements at high densities in order to solidify κ in the $B \propto \rho^{\kappa}$ relation; and (*c*) additional studies of the magnetic field morphology and strength both within cores and between cores and between GMCs.
3. The future will move toward much more comprehensive comparisons between observations and theory. Simulations with a variety of starting conditions will be observed in the computer at different evolutionary stages to produce images convolved with telescope instrumental signatures of dust polarization at multiple wavelengths and Zeeman and GK maps in various spectral lines. This approach should lead to resolution of many of the ambiguities that have plagued our understanding of magnetic fields in the formation of molecular clouds and their evolution into stars.

DISCLOSURE STATEMENT

The author is not aware of any affiliations, memberships, funding, or financial holdings that might be perceived as affecting the objectivity of this review.

ACKNOWLEDGMENTS

The author thanks S. Basu, E. Falgarone, C. Gammie, C. Heiles, M. Houde, A. Kemball, A. Lazarian, G. Novak, and T. Troland for critically reading an earlier version of this manuscript and providing comments that improved it. The author received funding support from the National Science Foundation under cooperative agreement AST0838226 and grant AST1007713.

LITERATURE CITED

Alcolea J, Menten KM, Moran JM, Reid MJ. 1993. *Lect. Notes Phys.* 412:225
Attard M, Houde M, Novak G, Li H-B, Vaillancourt JE, et al. 2009. *Ap. J.* 702:1584
Basu S, Ciolek GE, Wurster J. 2009. *New Astron.* 14:221
Bourke TL, Myers PC, Robinson G, Hyland AR. 2001. *Ap. J.* 554:916
Caswell JL, Kramer BH, Reynolds JE. 2011. *MNRAS* 414:1914
Chandrasekhar S, Fermi E. 1953. *Ap. J.* 118:113
Chapman NL, Goldsmith PF, Pineda JL Clemes DP, Li D, Krčo M. 2011. *Ap. J.* 741:21
Ciolek GE, Basu S. 2000. *Ap. J.* 529:925
Cortes PC, Crutcher RM, Matthews BC. 2006. *Ap. J.* 650:246
Cortes PC, Crutcher RM, Shepherd DS, Bronfman L. 2008. *Ap. J.* 676:464
Cortes PC, Crutcher RM, Watson WD. 2005. *Ap. J.* 628:780
Crutcher RM. 1979. *Ap. J.* 234:881
Crutcher RM. 1999. *Ap. J.* 520:706
Crutcher RM. 2004. *Ap. Space Sci.* 292:225
Crutcher RM, Evans NJ II, Troland T, Heiles C. 1975. *Ap. J.* 198:91
Crutcher RM, Hakobian N, Troland TH. 2009. *Ap. J.* 692:844
Crutcher RM, Hakobian N, Troland TH. 2010. *MNRAS* 402:64
Crutcher RM, Kazès I. 1983. *Astron. Astrophys.* 125:L23
Crutcher RM, Mouschovias TCh, Troland TH, Ciolek GE. 1994. *Ap. J.* 427:839
Crutcher RM, Troland TH. 2008. *Ap. J.* 685:281
Crutcher RM, Troland TH, Goodman AA, Heiles C, Kazès I, Myers PC. 1993. *Ap. J.* 407:175
Crutcher RM, Troland TH, Lazareff B, Kazès I. 1996. *Ap. J.* 456:217
Crutcher RM, Troland TH, Lazareff B, Paubert G, Kazès I. 1999. *Ap. J.* 514:121
Crutcher RM, Wandelt B, Heiles C, Falgarone E, Troland TH. 2010. *Ap. J.* 725:466
Cudlip W, Furniss I, King KJ, Jennings RE. 1982. *MNRAS* 200:1169
Curran RL, Chrysostomou A. 2007. *MNRAS* 382:699
Deguchi S, Watson WD. 1984. *Ap. J.* 285:126
Dennison B, Ward DB, Gull GE, Harwitt M. 1977. *Astron. J.* 82:39
Dotson JL, Vaillancourt JE, Kirby L, Dowell CD, Hildebrand RH, Davidson JA. 2010. *Ap. J. Suppl.* 186:406
Elmegreen BG. 2000. *Ap. J.* 530:277
Falceta-Gonçalves D, Lazarian A, Houde M. 2010. *Ap. J.* 713:1376
Falceta-Gonçalves D, Lazarian A, Kowal G. 2008. *Ap. J.* 679:537
Falgarone E, Troland TH, Crutcher RM, Paubert G. 2008. *Astron. Astrophys.* 487:247
Fish VL, Reid MJ, Argon AL, Menten KM. 2003. *Ap. J.* 596:328
Fish VL, Sjouwerman L. 2007. *Ap. J.* 668:331
Garcia-Barreto JA, Burke BF, Reid MJ, Moran JM, Haschick AD, Schilizzi RT. 1988. *Ap. J.* 326:954
Girart JM, Crutcher RM, Rao R. 1999 *Ap. J.* 525:L109
Girart JM, Greaves JS, Crutcher RM, Lai S-P. 2004. *Ap. Space Sci.* 292:119
Girart JM, Rao R, Marrone DP. 2006. *Science* 313:812
Glenn J, Walker CK, Bieging JH, Jewell PR. 1997. *Ap. J.* 487:L89
Goldreich P, Kylafis ND. 1981. *Ap. J.* 243:L75
Goldreich P, Sridhar S. 1995. *Ap. J.* 438:763
Goodman AA, Bastien P, Myers PC, Ménard F. 1990. *Ap. J.* 359:363

Goodman AA, Jones TJ, Lada E, Myers PC. 1995. *Ap. J.* 448:748
Gray MD, Field D. 1995. *Astron. Astrophys.* 298:243
Greaves JS, Holland WS, Dent WRF. 2002. *Ap. J.* 578:224
Greaves JS, Holland WS, Friberg P, Dent WRF. 1999. *Ap. J.* 512:L139
Greaves JS, Holland WS, Ward-Thompson D. 2001. *Ap. J.* 546:L53
Guilloteau S, Stier MT, Downes D. 1983. *Astron. Astrophys.* 126:10
Heiles C. 2000. *Astron. J.* 119:923
Heiles C, Crutcher RM. 2005. *Cosmic Magn. Fields*, ed. R Wielebinski, R Beck, pp. 137–82. Berlin: Springer
Heiles C, Troland TH. 2003. *Ap. J.* 586:106
Heiles C, Troland TH. 2004. *Ap. J. Suppl.* 151:271
Heiles C, Troland TH. 2005. *Ap. J.* 624:773
Heitsch F, Zweibel EG, Mac Low M-M, Li PS, Norman ML. 2001. *Ap. J.* 561:800
Hildebrand RH, Dragovan M, Novak G. 1984. *Ap. J.* 284:L51
Hildebrand RH, Kirby L, Dotson JL, Houde M, Vaillancourt JE. 2009. *Ap. J.* 696:567
Hiltner WA. 1949. *Science* 109:165
Hoang T, Lazarian A. 2008. *MNRAS* 388:117
Houde M, Bastien P, Dotso JL, Dowell CD, Hildebrand RH, et al. 2002. *Ap. J.* 569:803
Houde M, Bastien P, Peng R, Phillips TG, Yoshida H. 2000a. *Ap. J.* 536:857
Houde M, Peng R, Phillips TG, Bastien P, Yoshida H. 2000b. *Ap. J.* 537:245
Houde M, Peng R, Yoshida H, Hildebrand RH, Phillips TG, et al. 2004. *Ap. Space Sci.* 292:127
Houde M, Rao R, Vaillancourt JE, Hildebrand RH. 2011. *Ap. J.* 733:109
Houde M, Vaillancourt JE, Hildebrand RH, Chitsazzadeh S, Kirby L. 2009. *Ap. J.* 706:1504
Hurka JD, Schmid-Burgk J, Hardee PE. 1999. *Astron. Astrophys.* 343:558
Johnstone D, Boonman AMS, van Dishoeck EF. 2003. *Astron. Astrophys.* 412:157
Kirby L. 2010. *Ap. J.* 694:1056
Koch PM, Tang Y-W, Ho PTP. 2012. *Ap. J.* In press (arXiv:1201.4263v1)
Kudoh T, Basu S. 2008. *Ap. J.* 679:L97
Kwon W, Looney LW, Crutcher RM, Kirk JM. 2006. *Ap. J.* 653:1358
Kylafis ND. 1983. *Ap. J.* 275:135
Lai S-P, Crutcher RM, Girart JM, Rao R. 2001. *Ap. J.* 561:864
Lai S-P, Crutcher RM, Girart JM, Rao R. 2002. *Ap. J.* 566:925
Lai S-P, Girart JM, Crutcher RM. 2003. *Ap. J.* 598:392
Lazarian A. 2005. *AIP Conf. Proc.* 784:42
Lazarian A. 2007. *J. Quant. Spectrosc. Radiat. Transf.* 106:225
Lazarian A, Vishniac ET, Cho J. 2004 *Ap. J.* 603:180
Li H, Dowell CD, Goodman A, Hildebrand R, Novak G. 2009. *Ap. J.* 704:891
Li H, Griffin GS, Krejny M, Novak G, Loewenstein RF, et al. 2006. *Ap. J.* 648:340
Li H, Houde M. 2008. *Ap. J.* 677:1151
Lunttila T, Padoan P, Juvela M, Nordlund Å. 2009. *Ap. J.* 702:L37
MacLow M-M, Klessen RS. 2004. *Rev. Mod. Phys.* 76:125
MacLow M-M, Smith MD, Klessen RS, Burkert A. 1998. *Ap. Space Sci.* 261:195
Matthews BC, McPhee CA, Fissel LM, Curran RL. 2009. *Ap. J. Suppl.* 182:143
McKee CF, Ostriker EC. 2007. *Annu. Rev. Astron. Astrophys.* 45:565
Mestel L. 1966. *MNRAS* 133:265
Mouschovias TCh. 1991. In *The Physics of Star Formation and Early Stellar Evolution*, NATO ASIC Proc. 342, ed. CJ Lada, ND Kylafis, p. 61. Dordrecht: Kluwer
Mouschovias TCh, Ciolek GE. 1999. In *The Origin of Stars and Planetary Systems*, ed. CJ Lada, ND Kylafis, p. 305. Dordrecht: Kluwer
Mouschovias TCh, Tassis K. 2009. *MNRAS* 400:15
Mouschovias TCh, Tassis K. 2010. *MNRAS* 409:801
Nakamura F, Li Z-Y. 2005. *Ap. J.* 631:411
Nakano T, Nakamura T. 1978. *Publ. Astron. Soc. Jpn.* 30:681
Novak G, Dotson JL, Li H. 2009. *Ap. J.* 695:1362

Ostriker EC, Stone JM, Gammie CF. 2001. *Ap. J.* 546:980
Padoan P, Jimenez R, Juvela M, Nordlund Å. 2004. *Ap. J.* 604:L49
Padoan P, Nordlund Å. 1999. *Ap. J.* 526:279
Parker EN. 1957. *J. Geophys. Res* 62:509
Rao R, Crutcher RM, Plambeck RL, Wright MCH. 1998. *Ap. J.* 502:L75
Rees MJ. 2005. In *Cosmic Magn. Fields*, ed. R Wielebinski, R Beck, pp. 1–8. Berlin: Springer
Reid MJ, Haschick AD, Burke BF, Moran JM, Johnston KJ, Swenson GW. 1980. *Ap. J.* 239:89
Reid MJ, Silverstein EM. 1990. *Ap. J.* 361:483
Robishaw T. 2008. *Magnetic fields near and far: galactic and extragalactic single-dish radio observations of the Zeeman effect.* PhD thesis. Univ. Calif., Berkeley. 143 pp.
Shu FH, Adams FC, Lizano S. 1987. *Annu. Rev. Astron. Astrophys.* 25:23
Sweet PA. 1958. In *IAU Symp. 6, Electromagnetic Phenomena in Cosmical Physics*, ed. B Lehnert, p. 123. Cambridge, UK: Cambridge Univ. Press
Tassis K, Dowell CD, Hildebrand RH, Kirby L, Vaillancourt JE. 2009. *MNRAS* 399:1681
Troland TH, Crutcher RM. 2008. *Ap. J.* 680:457
Tilley DA, Balsara D. 2010. *MNRAS* 406:1201
Tilley DA, Pudritz RE. 2007. *MNRAS* 382:73
Turner BE, Gammon RH. 1975. *Ap. J.* 198:71
Vaillancourt JE, Dowell CD, Hildebrand R, Kirby L, Krejny M, et al. 2008. *Ap. J.* 679:L25
Vázquez-Semadeni E, Banerjee R, Gómez GC, Hennebelle P, Duffin D, Klessen RS. 2011. *MNRAS* 414:2511
Verschuur G. 1968. *Phys. Rev. Lett.* 21:775
Vlemmings WHT. 2007. *Proc. IAU Symp.* 242:37
Vlemmings WHT, Harvey-Smith L, Cohen RJ. 2006. *MNRAS* 371:L26
Vlemmings WHT, Torres RM, Dodson R. 2011. *Astron. Astrophys.* 529:A95
Wannier PG, Scoville NZ, Barvainis R. 1983. *Ap. J.* 267:126
Watson WD. 2009. *Rev. Mex. Astron. Astrofis.* 36:113
Wilner DJ, Reid MJ, Menten KM. 1999. *Ap. J.* 513:775
Wright MM, Gray MD, Diamond PJ. 2004a. *MNRAS* 350:1253
Wright MM, Gray MD, Diamond PJ. 2004b. *MNRAS* 350:1272
Wright MM, Gray MD, Diamond PJ. 2005. *MNRAS* 357:800
Wolleben M, Reich W. 2004. *Astron. Astrophys.* 427:537
Zweibel E. 1988. *Ap. J.* 329:384

Annual Review of Astronomy and Astrophysics

Volume 50, 2012

Contents

Indexes

Errata

An online log of corrections to *Annual Review of Astronomy and Astrophysics* articles may be found at http://astro.annualreviews.org/errata.shtml